CRYSTAL GROWTH & DESIGN

Article

pubs.acs.org/crystal

Organocounterions-Assisted and pH-Controlled Self-Assembly of Five Nanoscale High-Nuclear Lanthanide Substituted Heteropolytungstates

Yajie Liu,[†] Hailou Li,[†] Changtong Lu,[†,‡] Peijun Gong,[†] Xiaoyun Ma,[†] Lijuan Chen,*[,†] and Junwei Zhao*[,†]

[†]Henan Key Laboratory of Polyoxometalate Chemistry, Institute of Molecular and Crystal Engineering, College of Chemistry and Chemical Engineering, Henan University, Kaifeng, Henan 475004, People's Republic of China

[‡]China Tobacoo Henan Industrial Co. Ltd., Zhengzhou, Henan 450000, People's Republic of China

Supporting Information

ABSTRACT: Five high-nuclear lanthanide (Ln) substituted heteropolytungstates $[H_2N(CH_3)_2]_{16}Na_9LnH_{10}\{[W_{16}Ln_{10}(H_2O)_{38}O_{50}][B\text{-}\alpha\text{-}SeW_9O_{33}]_8\}\cdot 56H_2O$ [Ln = La^{III} (**1**), Ce^{III} (**2**)], $[H_2N(CH_3)_2]_{22}Na_4H_{12}\{[W_{18}Ln_{10}(H_2O)_{34}O_{56}][B\text{-}\alpha\text{-}SeW_9O_{33}]_8\}\cdot 80H_2O$ [Ln = La^{III} (**3**), Ce^{III} (**4**)], and $Na_4[H_2N(CH_3)_2]_{18}H_{21}[Nd(H_2O)_7][W_{16}Nd_{10}O_{50}(H_2O)_{34}(B\text{-}\alpha\text{-}AsW_9O_{33})_8]\cdot 60H_2O$ (**5**) were prepared by reaction of $Na_2WO_4\cdot 2H_2O$ and $Ln(NO_3)_3\cdot 6H_2O$ in the presence of dimethylamine hydrochloride (DMAHC) and Na_2SeO_3 or $NaAsO_2$ in an aqueous medium. The octameric polyoxoanions $\{[W_{16}Ln_{10}(H_2O)_{38}O_{50}][B\text{-}\alpha\text{-}SeW_9O_{33}]_8\}^{38-}$ in **1** and **2** are assembled from eight $[B\text{-}\alpha\text{-}SeW_9O_{33}]^{8-}$ building blocks linked by 16 extra bridging W^{VI} centers and ten Ln^{III} cations, whereas the octameric polyoxoanions $\{[W_{18}Ln_{10}(H_2O)_{34}O_{56}][B\text{-}\alpha\text{-}SeW_9O_{33}]_8\}^{38-}$ in **3** and **4** are constructed from eight $[B\text{-}\alpha\text{-}SeW_9O_{33}]^{8-}$ building blocks joined by 18 additional bridging W^{VI} centers and ten Ln^{III} cations [Ln = La^{III} (**3**), Ce^{III} (**4**)]. The octameric polyoxoanion $[W_{16}Nd_{10}O_{50}(H_2O)_{34}(B\text{-}\alpha\text{-}AsW_9O_{33})_8]^{40-}$ in **5** is constituted by eight $[B\text{-}\alpha\text{-}AsW_9O_{33}]^{9-}$ building blocks connected by 16 extra bridging W^{VI} centers and ten Nd^{III} cations. It should be noted that neighboring $\{[W_{16}Nd_{10}(H_2O)_{38}O_{50}][B\text{-}\alpha\text{-}AsW_9O_{33}]_8\}^{46-}$ polyoxoanions in **5** are further polymerized by two W−O−Nd−O−W linkers into a 1-D chain-like alignment. The thermolysis processes of **1**, **4**, and **5** were investigated by variable-temperature IR spectra, coloration changes, and variable-temperature PXRD patterns. The solid-state NIR luminescence properties of **5** were systematically studied at room temperature.

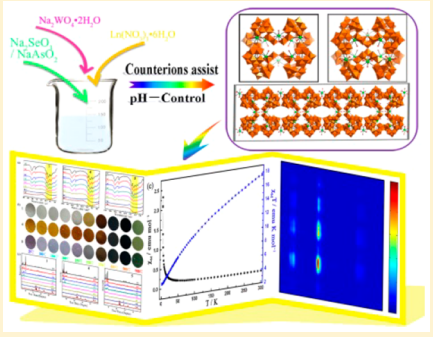

INTRODUCTION

Polyoxometalates (POMs), as an abundant and venerable class of metal-oxo-cluster-based compounds with nucleophilic oxygen-enrich surfaces, can serve as one of the outstanding inorganic polydentate ligands to chelate various metal ions, often leading to remarkably complicated nanoscale architectures with latent applications in different domains such as medicine, materials science, optics, catalysis, etc.[1−5] Among the POM field, it is well-known that heteropolyoxometalates (HPOMs) are the largest and most important subfamily and have drawn increasing attention in recent years on account of abundant structural topologies and interesting properties. Over the past two decades, the extensive explorations and discoveries on novel HPOM derivatives have been largely performed because the preformed lacunary POM clusters can highly encapsulate additional transition-metal (TM) or lanthanide (Ln) ions to construct diverse large POM aggregates.[6] Up to now, the rapid developments of TM-encapsulate HPOMs (TMEHPOMs) have been made, and some impressive examples have been already reported such as wheel-shaped $[Cu_{20}Cl(OH)_{24}(H_2O)_{12}(P_8W_{48}O_{184})]^{25-}$,[7] λ-shaped $[H_4CoWO(H_2O)_3(Se_2W_{26}O_{85})(Se_2W_{30}O_{107})_2]^{40-}$,[8] planar $\{Mn_{19}(OH)_{12}\}^{26+}$-incorporated $[Mn_{19}(OH)_{12}(SiW_{10}O_{37})_6]^{34-}$,[9] and gigantic Zr_{24}-cluster-substituted $[Zr_{24}O_{22}(OH)_{10}(H_2O)_2(W_2O_{10}H)_2(GeW_9O_{34})_4(GeW_8O_{31})_2]^{32-}$.[10] Moreover, encouraging achievements on Ln-encapsulated HPOMs (LEHPOMs) have been also made due to the potentials in optics, electricity, and magnetism resulting from the electronic and structural features of Ln ions.[11] For example, in 2009, Wang's group studied the electrochemical and electrocatalytic properties of a triple Dawson-type POM $[Ce_3^{IV}Mn_2^{IV}O_6(OAc)_6(H_2O)_9]_2[Mn_2^{III}P_2W_{16}O_{60}]_3^{20-}$.[12] In 2012, Huang and collaborators discovered that $\{[Sm(H_2O)_4(pdc)]_3\}\{[Sm(H_2O)_3(pdc)]\}[SiMo_{12}O_{40}]\cdot 3H_2O$ can show the good photocatalytic degradation activity toward rhodamine B.[13] In 2016, our group reported a class of trigonal pyramidal $\{AsO_2(OH)\}$-bridging LEHPOMs $\{[W_3Ln_2(H_2O)_8AsO_8(OH)][B\text{-}\alpha\text{-}AsW_9O_{33}]_2\}_2^{16-}$ (Ln = Eu^{III}, Gd^{III}, Tb^{III}, Dy^{III}, Ho^{III}) and probed their solid-state photoluminescence behaviors at room temperature.[14] Subsequently, Niu et al. reported a series of mono-Ln substituted inorganic−

Received: April 16, 2017
Revised: May 16, 2017
Published: June 8, 2017

DOI: 10.1021/acs.cgd.7b00539
Cryst. Growth Des. 2017, 17, 3917−3928

organic hybrids $[(\alpha\text{-}PW_{11}O_{39})Ln(C_4H_2O_6)]_2^{16-}$ (Ln = Dy^{III}, Er^{III}, Yb^{III}), and $[(\alpha\text{-}PW_{11}O_{39})Dy(C_4H_2O_6)]_2^{16-}$ represents a rare POM-based multifunctional material combining switchable luminescence, reversible photochromic, and single-molecule magnet properties.[15] Such low-nuclear LEHPOMs have been widely addressed previously, in contrast, the researches on high-nuclear LEHPOMs (HNLEHPOMs) with eight or more Ln centers are very limited. To the best of our knowledge, the pioneering work on HNLEHPOMs has been opened by Pope et al. in 1997 with a discovery of a water-soluble nanoscale polyoxoanion $[As_{12}Ce_{16}(H_2O)_{36}W_{148}O_{524}]^{76-}$ incorporating 12 $[B\text{-}\alpha\text{-}As^{III}W_9O_{33}]^{9-}$ units, four $[W_5O_{18}]^{6-}$ groups, and 16 Ce^{3+} centers.[16] However, it was not until 2007 that Kortz's group separated a 20-Ce^{III}-containing 100-tungsto-10-germanate $[Ce_{20}Ge_{10}W_{100}O_{376}(OH)_4(H_2O)_{30}]^{56-}$ by reaction of the trivacant precursor $[\alpha\text{-}GeW_9O_{34}]^{10-}$ and the Ce^{3+} ion.[17] From then on, the continuous interest in exploring HNLEHPOMs has been inspired and the pace of discovering novel HNLEHPOMs begins to accelerate. The groups of Hussain, Boskovic, and Patzke have demonstrated that the versatile precursor $[As_2W_{19}O_{67}(H_2O)]^{14-}$ is a useful candidate in constructing novel HNLEHPOMs such as octa-Gd^{III} bridging polytungstoarsenate $[Gd_8As_{12}W_{124}O_{432}(H_2O)_{22}]^{60-}$,[18] polynuclear Tb^{III} inorganic−organic hybrid $[Tb_8(pic)_6(H_2O)_{22}(B\text{-}\beta\text{-}AsW_8O_{30})_4(WO)_2(pic)_6]^{12-}$,[19] and hexadecameric $[Ln_{16}As_{16}W_{164}O_{576}(OH)_8(H_2O)_{42}]^{80-}$ (Ln = Eu^{III}, Gd^{III}, Tb^{III}, Dy^{III}, Ho^{III}).[20] Moreover, in 2009, a giant decanuclear HPOM $[Yb_{10}As_{10}W_{88}O_{308}(OH)_8(H_2O)_{28}(OAc)_4]^{40-}$ with additional acetate ligands bridging both Yb^{III} and W^{VI} centers was also obtained by Boskovic's group by means of the $[B\text{-}\alpha\text{-}AsW_9O_{33}]^{9-}$ precursor.[21] Later, Powell et al. reported a giant tetrahedral HNLEHPOM $[\{(GeW_9O_{34})_2Dy_3(\mu_2\text{-}OH)_3(H_2O)_2\}_6\{Co_2Dy_3(\mu_3\text{-}OH)_6(H_2O)_6\}_4]^{56-}$ using a one-pot self-assembly procedure in aqueous solution.[22] Very recently, Niu and co-workers communicated an unprecedented Ce_{10}-cluster-embedded POM $\{[Ce^{IV}{}_7Ce^{III}{}_3O_6(OH)_6(CO_3)(H_2O)_{11}][(P_2W_{16}O_{59})]_3\}^{19-}$ through a coordination-driven self-assembly strategy.[23] It should be pointed out that most of the above-mentioned HNLEHPOMs are made by using precursors such as $[\alpha\text{-}GeW_9O_{34}]^{10-}$, $[As_2W_{19}O_{67}(H_2O)]^{14-}$, $[B\text{-}\alpha\text{-}AsW_9O_{33}]^{9-}$, $[P_2W_{15}O_{56}]^{12-}$, etc., by the stepwise assembly strategy. However, to date, only a few HNLEHPOMs were synthesized through a straightforward one-step self-assembly reaction of simple staring materials,[16,24−27] although the stepwise assembly strategy has been viewed as a very effective method to prepare novel large poly(POM) aggregates.[28,29] Thus, it is clearly seen that the elaborate design and continuous synthesis of HNLEHPOMs by the one-step self-assembly reaction of simple staring materials remain a great challenge, which gives us a great impetus to explore this domain.

During the course of searching for novel HNLEHPOMs, we find that lone-electron-pair containing heteroatoms (such as As^{III}, Se^{IV}, etc.) can effectively prevent the formation of the plenary Keggin-type POM clusters and can make the Keggin-type POM clusters remain the lacunary modes, which allows extraneous Ln cations to incorporate into the lacunary POM matrixes or combine lacunary POM fragments together to give rise to unique HNLEHPOM architectures.[30,31] Inspired by this research background, recently, we have been concentrated on constructing novel high-nuclear Ln-containing selenotungstates and arsenotungstates based on Se^{IV} and As^{III} heteroatoms through the one-step self-assembly reaction of simple starting materials. We also found that dimethylamine hydrochloride (DMAHC) could play an important role in the assembly process of HNLEHPOMs. On one hand, in the acidic solution, dimethylamine components can be protonated to form organic cations, and protonated dimethylamine cations can effectively hamper Ln ions from forming precipitates in the tungstate system, further improving the coordination ability of Ln ions with in situ formed lacunary HPOM fragments, which allows for the construction of novel HNLEHPOMs with novel structures. However, considering that protonated dimethylamine cations have the larger cation radius in contrast to Na^+ or K^+ cations, therefore, protonated dimethylamine cations can be more suitable to work as the charge balance cations to stabilize the resulting HNLEHPOMs. It is well-known that the pH control is a significant influential factor in the formation of various POMs,[32−34] as a result, the pH-dependent synthetic approach should be considered in synthesizing HNLEHPOMs. Based on the above ideas, we utilized the pH-dependent one-step self-assembly strategy of sodium tungstate reacting with Ln ions and heteroatom (Se^{IV}, As^{III}) ingredients in the presence of DMAHC to prepare two classes of protonated dimethylamine balanced HNLEHPOMs $[H_2N(CH_3)_2]_{16}Na_9LnH_{10}\{[W_{16}Ln_{10}(H_2O)_{38}O_{50}][B\text{-}\alpha\text{-}SeW_9O_{33}]_8\}\cdot 56H_2O$ [Ln = La^{III} (**1**), Ce^{III} (**2**)] and $[H_2N(CH_3)_2]_{22}Na_4H_{12}\{[W_{18}Ln_{10}(H_2O)_{34}O_{56}][B\text{-}\alpha\text{-}SeW_9O_{33}]_8\}\cdot 80H_2O$ [Ln = La^{III} (**3**), Ce^{III} (**4**)]. To our knowledge, **1**−**4** are the infrequent octameric selenotungstates based on trivacant $[B\text{-}\alpha\text{-}SeW_9O_{33}]^{8-}$ building blocks and additional W and Ln connectors. It should be pointed out that the different pH values of the reaction system lead to the formation of **1**−**4**. When the pH was adjusted to 3.0, **1** and **2** were made; on the contrast, when the pH was set to 4.0, **3** and **4** were found. Under the similar reaction conditions of **3** and **4**, we found a 1-D chain high-nuclear Nd-containing arsenotungstate $[H_2N(CH_3)_2]_{18}Na_4H_{21}[Nd(H_2O)_7][W_{16}Nd_{10}O_{50}(H_2O)_{34}(B\text{-}\alpha\text{-}AsW_9O_{33})_8]\cdot 60H_2O$ (**5**) established by Nd_{10}-comprising $\{[W_{18}Nd_{10}(H_2O)_{34}O_{56}][B\text{-}\alpha\text{-}AsW_9O_{33}]_8\}^{46-}$ cluster anions and Nd^{III} linkers. Remarkably, such 1-D chain-like motif is observed for the first time among the octameric LEHPOMs. Moreover, the thermal stability properties of **1**, **4**, and **5** were comparatively deeply studied by variable-temperature PXRD spectra, variable-temperature IR spectra, and color changes of the samples. The magnetic susceptibility measurements for **2**, **4**, and **5** were performed. Also, the NIR photoluminescence spectrum and the lifetime decay behavior of **5** were conducted. The time-resolved luminescence spectrum measurements indicate no occurrence of the intramolecular energy transfer of the oxygen-to-metal (O → W) charge-transfer transitions sensitizing the emission of Nd^{III} cations in **5** in the NIR region.

EXPERIMENTAL SECTION

Materials and Methods. All the reagents needed for the synthesis are of analytical grade and are used as purchased. C, H, and N analyses were carried out on a Vario EL Cube CHNS analyzer. Inductively coupled plasma atomic emission spectrometry (ICP-AES) was performed on a Perkin−Elmer Optima 2000 ICP-AES spectrometer. IR spectra were collected with a PerkinElmer FT-IR spectrometer in a KBr plate in the range of 400−4000 cm^{-1}. PXRD patterns were recorded on a Bruker D8 ADVANCE apparatus with Cu Kα radiation (λ = 1.54056 Å) at 293 K. Thermogravimetric (TG) analyses were measured under a N_2 atmosphere on a Mettler−Toledo TGA/SDTA 851^e instrument at a heating rate of 10 °C·min^{-1} from 25 to 1000 °C. The magnetic experiments were measured on a Quantum Design MPMS XL 7 SQUID magnetometer. Photoluminescence spectra and lifetimes were recorded using an FLS 980 Edinburgh Analytical Instrument furnished by a 450 W xenon lamp and a μF900H high-energy microsecond flash lamp as the excitation sources.

DOI: 10.1021/acs.cgd.7b00539
Cryst. Growth Des. 2017, 17, 3917−3928

Table 1. Crystallographic Data and Structure Refinements for 1−5

	1	2	3	4	5
empirical formula	$C_{32}H_{326}La_{11}N_{16}Na_9O_{408}Se_8W_{88}$	$C_{32}H_{326}Ce_{11}N_{16}Na_9O_{408}Se_8W_{88}$	$C_{44}H_{416}La_{10}N_{22}Na_4O_{434}Se_8W_{90}$	$C_{44}H_{416}Ce_{10}N_{22}Na_4O_{434}Se_8W_{90}$	$C_{36}H_{367}Nd_{11}N_{18}Na_4O_{415}As_8W_{88}$
formula weight	26010.49	26023.80	26859.23	26871.33	26151.24
crystal system	triclinic	triclinic	triclinic	triclinic	triclinic
space group	$P\bar{1}$	$P\bar{1}$	$P\bar{1}$	$P\bar{1}$	$P\bar{1}$
a, Å	20.6965(12)	20.626(2)	20.639(2)	20.525(3)	18.9946(13)
b, Å	24.8575(15)	24.813(3)	24.920(3)	24.793(4)	24.3271(16)
c, Å	29.1101(17)	29.044(3)	29.090(3)	28.922(4)	30.489(2)
α, deg	71.8320(10)	71.604(2)	71.648(2)	71.440(2)	102.1030(10)
β, deg	82.9870(10)	82.850(2)	83.031(2)	83.136(3)	97.7030(10)
γ, deg	69.2870(10)	69.108(2)	69.409(2)	69.145(3)	93.9650(10)
V, Å^{-3}	13308.6(14)	13176(3)	13292(3)	13038(3)	13582.2(16)
Z	1	1	1	1	1
μ, mm^{-1}	20.432	20.696	20.814	21.273	20.153
$F(000)$	11404	11415	11852	11862	11509
T, K	296(2)	296(2)	296(2)	296(2)	296(2)
limiting indices	$-20 \le h \le 24$	$-18 \le h \le 24$	$-24 \le h \le 21$	$-24 \le h \le 24$	$-22 \le h \le 22$
	$-29 \le k \le 29$	$-25 \le k \le 29$	$-29 \le k \le 25$	$-29 \le k \le 29$	$-21 \le k \le 28$
	$-34 \le l \le 34$	$-34 \le l \le 34$	$-34 \le l \le 34$	$-34 \le l \le 25$	$-36 \le l \le 34$
No. of reflections collected	69410	68128	68677	66685	70383
No. of independent reflections	46641	46115	46569	45572	47541
R_{int}	0.0774	0.0886	0.0846	0.0950	0.0662
data/restrains/parameters	46641/162/2211	46115/426/2216	46569/16/1432	45572/11/1439	47541/172/2150
GOF on F^2	1.021	0.945	1.004	1.027	1.047
final R indices [$I > 2\sigma(I)$]	$R_1 = 0.0738$	$R_1 = 0.0706$	$R_1 = 0.0797$	$R_1 = 0.0731$	$R_1 = 0.0665$
	$wR_2 = 0.1491$	$wR_2 = 0.1421$	$wR_2 = 0.1478$	$wR_2 = 0.1591$	$wR_2 = 0.1504$
R indices (all data)	$R_1 = 0.1596$	$R_1 = 0.1561$	$R_1 = 0.1917$	$R_1 = 0.1685$	$R_1 = 0.1323$
	$wR_2 = 0.1724$	$wR_2 = 0.1633$	$wR_2 = 0.1697$	$wR_2 = 0.2029$	$wR_2 = 0.1681$

*Synthesis of $[H_2N(CH_3)_2]_{16}Na_9LaH_{10}\{[W_{16}La_{10}(H_2O)_{38}O_{50}][B\text{-}\alpha\text{-}SeW_9O_{33}]_8\}\cdot 56H_2O$ (**1**).* $Na_2WO_4\cdot 2H_2O$ (1.000 g, 3.032 mmol), DMAHC (0.502 g, 6.156 mmol), and Na_2SeO_3 (0.050 g, 0.289 mmol) were successively dissolved in distilled water (20 mL). Then, the pH of the resulting solution was adjusted to 3.0 by using hydrochloric acid (6.0 mol·L^{-1}), $La(NO_3)_3\cdot 6H_2O$ (0.150 g, 0.346 mmol) was added, and the pH was again adjusted to 3.0. After stirring for 30 min, the resulting solution was filtered and left to slowly evaporate at room temperature, and colorless block crystals of **1** were obtained for several weeks. Yield: 0.36 g [40.5% based on $La(NO_3)_3\cdot 6H_2O$]. Anal. Calcd (Found %) for $C_{32}N_{16}H_{326}Na_9W_{88}La_{11}O_{408}Se_8$ (**1**): C 1.48 (1.63), H 1.26 (1.58), N 0.86 (0.94), Na 0.80 (0.84), Se 2.43 (2.59), W 62.20 (63.33), La 5.87 (5.64). IR (KBr, cm^{-1}): 3422 (s), 3162 (w), 2791 (w), 2427 (w), 2088 (w), 1628 (s), 1465 (s), 966 (s), 872 (vs), 789 (s), 742 (m), 647 (w), 482 (m) (Figure S1, Supporting Information).

*Synthesis of $[H_2N(CH_3)_2]_{16}Na_9CeH_{10}\{[W_{16}La_{10}(H_2O)_{38}O_{40}][B\text{-}\alpha\text{-}SeW_9O_{33}]_8\}\cdot 56H_2O$ (**2**).* Compound **2** was synthesized following the procedure described for **1** but with $Ce(NO_3)_3\cdot 6H_2O$ (0.152 g, 0.350 mmol) instead of $La(NO_3)_3\cdot 6H_2O$. The yellow block crystals of **2** were isolated. Yield: 0.36 g [40.4% based on $Ce(NO_3)_3\cdot 6H_2O$]. Anal. Calcd (Found %) for $C_{32}N_{16}H_{326}Na_9W_{88}Ce_{11}O_{408}Se_8$ (**2**): C 1.48 (1.59), H 1.26 (1.60), N 0.86 (0.95), Na 0.80 (0.86), Se 2.43 (2.61), W 62.17 (63.21), Ce 5.92 (5.50). IR (KBr, cm^{-1}): 3462 (s), 3158 (w), 2790 (w), 2431 (w), 2084 (w), 1620 (s), 1463 (s), 970 (s), 865 (vs), 788 (s), 736 (m), 643 (w), 479 (m) (Figure S1, Supporting Information).

*Synthesis of $[H_2N(CH_3)_2]_{22}Na_4H_8\{[W_{18}La_{10}(H_2O)_{34}O_{56}][B\text{-}\alpha\text{-}SeW_9O_{33}]_8\}\cdot 90H_2O$ (**3**).* $Na_2WO_4\cdot 2H_2O$ (1.200 g, 3.638 mmol), DMAHC (0.502 g, 6.156 mmol) and Na_2SeO_3 (0.050 g, 0.289 mmol) were successively dissolved in 20 mL of distilled water. Then, the pH of the resulting solution was adjusted to 4.0 by the addition of dilute HCl (6.0 mol·L^{-1}). After that, $La(NO_3)_3\cdot 6H_2O$ (0.198 g, 0.457 mmol) was added, and the pH was again adjusted to 4.0. After stirring for 30 min, the resulting solution was filtered and left to slowly evaporate at ambient temperature. Colorless strip crystals of **3** were formed after several weeks. Yield: 0.42 g [34.2% based on $La(NO_3)_3\cdot 6H_2O$]. Anal. Calcd (Found %) for $H_{416}N_{22}C_{44}Na_4W_{90}La_{10}Se_8O_{434}$ (**3**): C 1.98 (2.06), H 1.56 (1.75), N 1.15 (1.22), Na 0.34 (0.48), Se 2.35 (2.58), W 61.60 (62.94), La 5.17 (5.03). IR (KBr, cm^{-1}): 3334 (s), 3158 (s), 2782 (w), 2437 (w), 2088 (w), 1619 (s), 1463 (s), 968 (s), 869 (vs), 789 (s), 738 (m), 652 (w), 486 (m) (Figure S1, Supporting Information).

*Synthesis of $[H_2N(CH_3)_2]_{22}Na_4H_{12}\{[W_{18}Ce_{10}(H_2O)_{34}O_{56}][B\text{-}\alpha\text{-}SeW_9O_{33}]_8\}\cdot 80H_2O$ (**4**).* The synthesis process of **4** is similar to that of **3** except that $La(NO_3)_3\cdot 6H_2O$ (0.198 g, 0.457 mmol) was replaced by $Ce(NO_3)_3\cdot 6H_2O$ (0.199 g, 0.458 mmol). The yellow strip crystals of **4** were isolated. Yield: 0.42 g [34.9% based on $Ce(NO_3)_3\cdot 6H_2O$]. Anal. Calcd (Found %) for $H_{416}N_{22}C_{44}Na_4W_{90}Ce_{10}Se_8O_{434}$ (**4**): C 1.97 (2.01), H 1.56 (1.76), N 1.14 (1.18), Na 0.34 (0.40), Se 2.35 (2.69), W 61.58 (62.10), Ce 5.21 (5.11). IR (KBr, cm^{-1}): 3422 (s), 3168 (w), 2790 (w), 2431 (w), 2084 (w), 1630 (s), 1467 (s), 970 (s), 875 (vs), 788 (s), 739 (m), 645 (w), 493 (m) (Figure S1, Supporting Information).

*Synthesis of $[H_2N(CH_3)_2]_{18}Na_4H_{21}[Nd(H_2O)_7][W_{16}Nd_{10}O_{50}(H_2O)_{34}\text{-}(B\text{-}\alpha\text{-}AsW_9O_{33})_8]\cdot 60H_2O$ (**5**).* $Na_2WO_4\cdot 2H_2O$ (1.400 g, 4.244 mmol) and DMAHC (0.501 g, 6.144 mmol) were dissolved in distilled water (20 mL) under magnetic stirring. Then, $NaAsO_2$ (0.5 mL, 1 mol·L^{-1}) was added. After the pH of the resulting solution was set at 4.0 using HCl (6.0 mol·L^{-1}), $Nd(NO_3)_3\cdot 6H_2O$ (0.199 g, 0.454 mmol) was added and the pH was again adjusted to 4.0. After stirring for 30 min, the solution was filtered and left to slowly evaporate at room temperature, and purple strip crystals of **5** were obtained for several weeks. Yield: 0.11 g [10.4% based on $Nd(NO_3)_3\cdot 6H_2O$]. Anal. Calcd (Found %) for $H_{367}C_{36}N_{18}O_{415}Na_4As_8Nd_{11}W_{88}$ (**1**): C 1.65 (1.88), H 1.41 (1. 80), N 0.96 (1.10), Na 0.35 (0.41), As 2.29 (2.18), W 61.87 (61.51), Nd 6.07 (6.24). IR (KBr, cm^{-1}): 3424 (s), 3157 (w), 2787 (w), 2450 (w), 2105 (w), 1629 (s), 1462 (s), 952 (s), 864 (vs), 782 (s), 714 (m), 642 (w), 481 (m) (Figure S1, Supporting Information).

DOI: 10.1021/acs.cgd.7b00539
Cryst. Growth Des. 2017, 17, 3917−3928

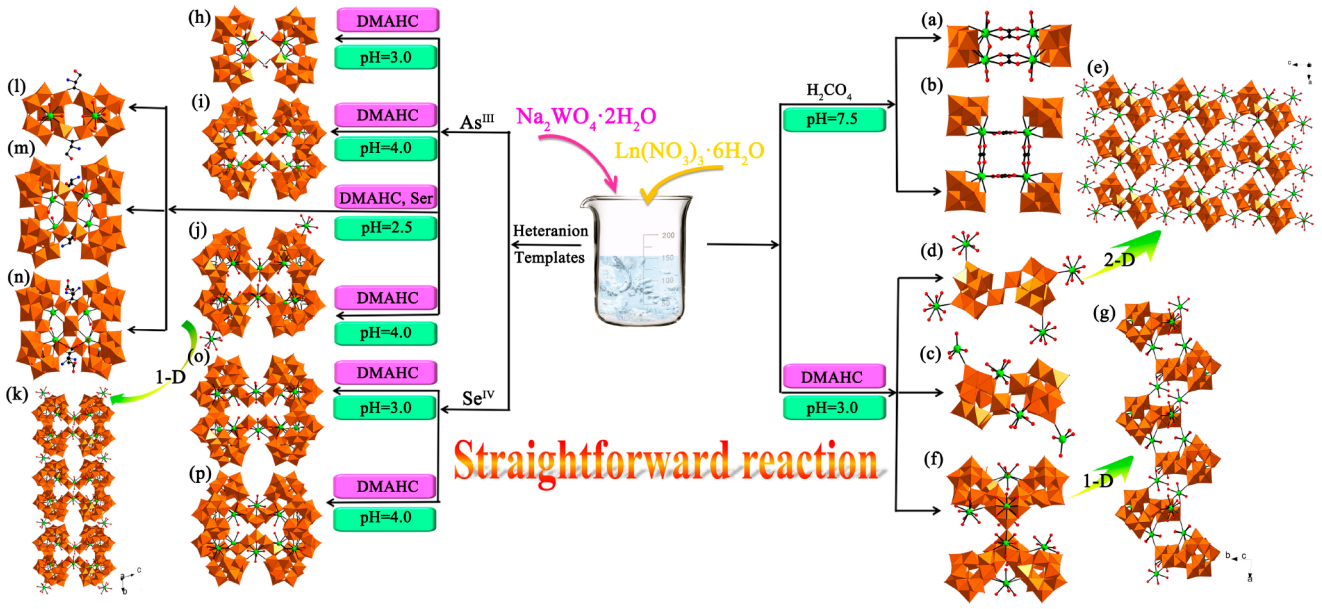

Figure 1. (a) Structural unit of double-oxalate-bridging dimer $\{[Ln_2(C_2O_4)(H_2O)_4(OH)W_4O_{16}]_2\}^{10-}$. (b) Structure of single-oxalate-bridging tetramer $\{[Ln(C_2O_4)W_5O_{18}]_4\}^{20-}$. (c) Molecular unit of $\{[Ln(H_2O)_4][Ln(H_2O)_5]_2[W_{22}O_{74}H_2]\}^{5-}$. (d,e) Molecular structural unit of $\{[Eu(H_2O)_7]_2[Eu(H_2O)_5]_2[W_{22}O_{74}H_2]\}^{2-}$ and its 2-D sheet structure. (f,g) Molecular structural unit of $\{[Ln_4(H_2O)_{22}W_{28}O_{94}H_2]\}^{12-}$ and its 1-D chain-like structure. (h) Structural unit of $\{AsO_2(OH)\}$ bridging tetranuclear arsenotungstate $\{[W_3Ln_2(H_2O)_8AsO_8(OH)][B\text{-}\alpha\text{-}AsW_9O_{33}]_2\}_2^{16-}$. (i) Structure unit of the nanosized octameric arsenotungstate $\{[[Ln_{10}W_{16}(H_2O)_{30}O_{50}(B\text{-}\alpha\text{-}AsW_9O_{33})_8]\}^{46-}$. (j,k) Molecular structural unit of **5** and its 1-D chain-like structure. (l) Structure of the dimeric arsenotungstate $[Ln_2W_4O_{10}(H_2O)_8(Ser)_2(B\text{-}\alpha\text{-}AsW_9O_{33})_2]^{9-}$. (m) Structure of the tetrameric arsenotungstate $[Ln_4W_8O_{19}(H_2O)_{10}(OH)_2(Ser)_2(B\text{-}\alpha\text{-}AsW_9O_{33})_4]^{16-}$. (n) Structure of the tetrameric arsenotungstate $[Ln_4W_8O_{19}(H_2O)_8(OH)_2(Ser)_4(B\text{-}\alpha\text{-}AsW_9O_{33})_4]^{16-}$. (o) Structure unit of isostructural **1**−**2**. (p) Structure unit of isostructural **3**−**4**.

X-ray Crystallography. In order to avoid efflorescence during the course of collecting intensity data, high-quality single crystals of **1**−**5** were selected from their mother liquors and sealed to glass tubes for X-ray crystal structure determination. X-ray diffraction data of **1**−**5** were collected on a Bruker APEX−II CCD diffractometer at 296(2) K with graphite monochromated Mo Kα radiation (λ = 0.71073 Å). Their structures were solved by direct methods by the SHELXTL−97 program package.[35,36] Lorentz polarization and empirical absorption corrections were applied. All H atoms were refined isotropically as a riding model using the default SHELXTL parameters. All the non-H atoms were refined anisotropically except for some O, C, and N atoms and some H_2O molecules. No H atoms linking to water molecules were located from the difference Fourier maps. According to the check cif reports of **1**−**5**, very large solvent accessible voids in their structures are found, which suggest that some counter cations and water molecules should exist in the structures that cannot be found from the weak residual electron peaks. Based on the charge-balance considerations and the results of elemental analyses and TG analyses, 12 protonated $[H_2N(CH_3)_2]^+$ cations and 20 lattice water molecules for **1** and **2**, four protonated $[H_2N(CH_3)_2]^+$ cations and thirty-eight lattice water molecules for **3** and **4**, and eight protonated $[H_2N(CH_3)_2]^+$ cations and 34 lattice water molecules for **5** were directly added to their molecular formulas. This phenomenon is very common in POM chemistry.[37] Crystallographic data and structural refinement parameters for **1**−**5** are listed in Table 1. The crystallographic data for the structures reported in this paper have been deposited in the Cambridge Crystallographic Data Centre with CCDC 1544230, 1544228, 1544229, 1544231, and 1544232 for **1**−**5**. These data can be also obtained free of charge from the Cambridge Crystallographic Data Centre via www.ccdc.cam.ac.uk/data_request/cif.

RESULTS AND DISCUSSION

Synthesis. Compounds **1**−**5** were isolated from a pH-dependent one-step self-assembly strategy of $Na_2WO_4{\cdot}2H_2O$, SeO_3^{2-}/AsO_3^{3-} and Ln cations in the presence of DMAHC in the aqueous solution. Since the first LEHPOM $(NH_4)_2[H_6CeMo_{12}O_{42}]{\cdot}nH_2O$ was discovered by Barbieri in 1914,[38] a large number of LEHPOMs have been obtained. Moreover, their latent applications have attracted widespread attention in the fields of magnetism, medicine, and fluorescence.[14,15,19,30,31] Considering the oxophile nature and multiple coordination requirements of Ln ions and the advantages of the one-step self-assembly reaction of simple staring materials, the aqueous system including $Na_2WO_4{\cdot}2H_2O$, $Ln(NO_3)_3{\cdot}6H_2O$, and various organic solubilizers have been explored by us since 2014 and some neoteric LEHPOMs were isolated. First, two types of interesting oxalate-bridging Ln-containing isopolyoxotungstate hybrids $[Ln_2(C_2O_4)(H_2O)_4(OH)W_4O_{16}]_2^{10-}$ (Figure 1a) and $[Ln(C_2O_4)W_5O_{18}]_4^{20-}$ (Ln = Eu^{III}, Ho^{III}, Er^{III}, Tb^{III}) (Figure 1b) were prepared.[39] It should be pointed out that the use of different alkaline cations induces the formation of two structural types. The former is synthesized when only Na^+ ions are used in the system, while the latter is acquired when mixed Na^+ and K^+ ions are simultaneously used. In an effort to explore the effect of organic cations, DMAHC was introduced to the system, and we obtained three types of Ln-containing isopolyoxotungstates of discrete $[Ln(H_2O)_4][Ln(H_2O)_5]_2[W_{22}O_{74}H_2]^{5-}$ (Ln = Gd^{III}, Tb^{III}, Er^{III}, Tm^{III}, Yb^{III}, Lu^{III}) (Figure 1c), 2-D network $[Eu(H_2O)_7]_2[Eu(H_2O)_5]_2[W_{22}O_{74}H_2]^{2-}$ (Figures 1d,e), and 1-D chain-like $[Ln_4(H_2O)_{22}W_{28}O_{94}H_2]_2^{12-}$ (Ln = Pr^{III}, Nd^{III}, Sm^{III}) (Figures 1f,g).[40] Recently, the lone-electron-pair containing heteroatom components (such as Se^{IV}, As^{III}, Sb^{III}, etc.) have demonstrated the great superiority in assembling distinctive POM architectures.[8,41,42] Moreover, recent studies indicate that the simultaneous utilization of Ln cations and the lone-electron-pair containing heteroatoms can favor to construct large LEHPOMs on account of the inducing effect of the lone pair of electrons located on heteroatoms.[25] This background provides us with an excellent opportunity to exploit the LEHPOM system.

DOI: 10.1021/acs.cgd.7b00539
Cryst. Growth Des. 2017, 17, 3917−3928

As a result, a class of trigonal pyramidal {$AsO_2(OH)$}-bridging Ln substituted arsenotungstates $\{[W_3Ln_2(H_2O)_8AsO_8(OH)][B\text{-}\alpha\text{-}AsW_9O_{33}]_2\}_2^{16-}$ (Ln = Eu^{III}, Gd^{III}, Tb^{III}, Dy^{III}, Ho^{III}) were isolated by reaction of $NaAsO_2$, $Ln(NO_3)_3{\cdot}6H_2O$, and $Na_2WO_4{\cdot}2H_2O$ in a molar ratio of 1.000:0.457:3.642 (Figure 1h), which is constituted by four trivacant Keggin $[B\text{-}\alpha\text{-}AsW_9O_{33}]^{9-}$ units linked via an elliptical $[W_6Ln_4(H_2O)_{16}As_2O_{16}(OH)_2]^{20+}$ moiety.[15] Although a large number of LEHPOMs have been already obtained to date, the design and preparation of HNLEHPOMs remain still a great challenge owing to the mechanism of formation is not well understood. Consequently, it is fairly difficult to search suitable reaction conditions that could capacitate the acquisition of novel HNLEHPOMs. Just so, an effective reaction strategy with the introduction of organic solubilizers such as DMAHC has been developed by us to overcome this difficulty. Simultaneously, in order to entail the reaction shift to the direction of the desired HNLEHPOMs, excess Ln cations were used in the reaction process. Under our unremitting exploration, when the reactant molar ratio of $NaAsO_2/Ln(NO_3)_3{\cdot}6H_2O/Na_2WO_4{\cdot}2H_2O$ was increased to 1.000:0.908:8.488, a series of nanosized HNLEHPOMs $\{[[Ln_{10}W_{16}(H_2O)_{30}O_{50}(B\text{-}\alpha\text{-}AsW_9O_{33})_8]\}^{46-}$ [Ln = Eu^{III}, Sm^{III}, Gd^{III}, Tb^{III}, Dy^{III}, Ho^{III}, Er^{III}, Tm^{III}] were successfully isolated by us (Figure 1i).[30] Unexpectedly, when we put $Nd(NO)_3{\cdot}6H_2O$ into this reaction system, another novel 1-D chain Nd-containing arsenotungstate **5** was made and is built by nanosized $[W_{16}Nd_{10}O_{50}(H_2O)_{34}(B\text{-}\alpha\text{-}AsW_9O_{33})_8]^{46-}$ clusters via $[Nd(H_2O)_7]^{3+}$ linkers (Figures 1j,k). Very recently, the reactant molar ratio was further improved by us in the presence of two organic solubilizers (DMAHC and Ser). To our surprise, when the reactant molar ratio was elevated to 1.000:0.880:18.200 and 1.000:1.760:18.20, three types of Ser-decorated LEHPOMs $[Ln_2W_4O_{10}(H_2O)_8(Ser)_2(B\text{-}\alpha\text{-}AsW_9O_{33})_2]^{9-}$ (Ln = Eu^{III}, Gd^{III}, Tb^{III}, Dy^{III}, Ho^{III}, Er^{III}, Tm^{III}, Yb^{III}) (Figure 1l), $[Ln_4W_8O_{19}(H_2O)_{10}(OH)_2(Ser)_2(B\text{-}\alpha\text{-}AsW_9O_{33})_4]^{16-}$ (Ln = Dy^{III}, Ho^{III}, Er^{III}, Yb^{III}, Tm^{III}) (Figure 1m), and $[Ln_4W_8O_{19}(H_2O)_8(OH)_2(Ser)_4(B\text{-}\alpha\text{-}AsW_9O_{33})_4]^{16-}$ (Ln = Ce^{III}, Pr^{III}, Nd^{III}, Sm^{III}, Eu^{III}) (Figure 1n) were synthesized (Ser = L-serine).[31] Considering the similarities between AsO_2^- and SeO_3^{2-}, the system containing WO_4^{2-}, SeO_3^{2-}, and Ln^{3+} ions was also investigated by us. Fortunately, four unique high-nuclear Ln-containing selenotungstates **1**−**4** were successfully obtained. It is worth noting that the pH plays a dominating role in the formation of **1**−**4**. When the pH of the reaction system was set at 3.0, **1** and **2** (Figure 1o) were obtained and both include a 26 W−Ln heterometal cluster $[W_{16}Ln_{10}(H_2O)_{38}O_{50}]^{26+}$ (Ln = La^{III}, Ce^{III}) stabilized by eight trivacant $[B\text{-}\alpha\text{-}SeW_9O_{33}]^{8-}$ building blocks. When we raised the pH to about 4.0, **3** and **4** (Figure 1p) were found and both consist of a 28 W−Ln heterometal cluster $[W_{18}Ln_{10}(H_2O)_{34}O_{56}]^{26+}$ (Ln = La^{III}, Ce^{III}) stabilized by eight trivacant $[B\text{-}\alpha\text{-}SeW_9O_{33}]^{8-}$ building blocks. From our reported results, several key points can be summarized as follows: (a) The choice of different counter cations can influence the structure diversity of POM fragments in the final products. The smaller Na^+ and K^+ cations lead to the formation of divacant Lindqvist $[W_4O_{16}]^{8-}$ and monovacant Lindqvist $[W_5O_{18}]^{6-}$. On contrast, when the larger protonated dimethylamine cation was used, the formation of larger POM fragments such as $[B\text{-}\alpha\text{-}AsW_9O_{33}]^{9-}$, $[W_{22}O_{74}H_2]^{14-}$, and $[W_{28}O_{94}H_2]^{18-}$ is favorable. It is worth mentioning that the use of DMAHC can inhibit the hydrolysis of Ln ions and also avert the overquick reaction and prevent the formation of quick precipitates between Ln ions and tungstates, which can greatly improve the coordinating ability of Ln ions in the system and induce the formation of larger POM fragments. (b) The nature of Ln cations can also influence the structural constructions of the final products. For example, La^{3+}, Ce^{3+}, and Pr^{3+} cations were used under the similar conditions to **5**; unfortunately, the parallelogram crystals $[LnNa(H_2O)_4(OH)WO(H_2O)(B\text{-}\alpha\text{-}AsW_9O_{33})_2]^{11-}$ (Ln = La^{III}, Ce^{III}, Pr^{III}) were obtained, which reveal the sandwich-type structure (Figure S2, Supporting Information).[43] When the Nd^{3+} cation was introduced to the system, **5** can be obtained. (c) The pH is also an important factor. For example, it is found that the optimal pH for the crystal growth for **5** is in the range of pH 3.8−4.2. However, when the pH was lower or higher than this range, no crystalline products were obtained. Moreover, the formation of **1**−**4** was chiefly also controlled by the pH. When the pH was adjusted to 3.0, the reaction solution is clear, which is favorable for the growth of **1**−**2**. When the pH was set at 4.0, the reaction solution became slightly cloudy and the evaporation of the filtrate led to the isolation of **3**−**4** after 10 days. In the future, we will persist in exploring much more HNLEHPOMs with novel architectures and excellent properties by controlling different synthetic conditions such as the reactant ratio, the nature of Ln cations, pH, temperature, and introduction of functional organic ligands.

Structural Description. Compounds **1**−**5** crystallize in the triclinic space group $P\bar{1}$. **1**−**4** adopt the discrete structure, whereas **5** employs the 1-D chain alignment. The polyoxoanionic skeletons of isostructural **1** and **2** exhibit an octameric aggregate $\{[W_{16}Ln_{10}(H_2O)_{38}O_{50}][B\text{-}\alpha\text{-}SeW_9O_{33}]_8\}^{38-}$ assembled from eight $[B\text{-}\alpha\text{-}SeW_9O_{33}]^{8-}$ building blocks linked by 16 extra bridging W^{VI} centers and ten Ln^{III} cations [Ln = La^{III} (**1**), Ce^{III} (**2**)], while the polyoxoanionic skeletons of isostructural **3** and **4** also exhibit an octameric assembly $\{[W_{18}Ln_{10}(H_2O)_{34}O_{56}][B\text{-}\alpha\text{-}SeW_9O_{33}]_8\}^{38-}$ constructed from eight $[B\text{-}\alpha\text{-}SeW_9O_{33}]^{8-}$ building blocks joined by 18 additional bridging W^{VI} centers and ten Ln^{III} cations [Ln = La^{III} (**3**), Ce^{III} (**4**)]. The molecular structural unit of **5** displays an octameric polyoxoanion $[W_{16}Nd_{10}O_{50}(H_2O)_{34}(B\text{-}\alpha\text{-}AsW_9O_{33})_8]^{40-}$ built by eight $[B\text{-}\alpha\text{-}AsW_9O_{33}]^{9-}$ building blocks connected by 16 extra bridging W^{VI} centers and ten Nd^{III} cations. Herein, the structures of only **1**, **3**, and **5** are discussed. The experimental PXRD patterns for **1**, **3**, and **5** are well consistent with the simulated XRD patterns from the single-crystal diffraction data, demonstrating the high phase purity of the samples used for the property measurements (Figure S3, Supporting Information). The intensity differences between the simulated and experimental XRD patterns primarily might be related to the variation in preferred orientation of the powder samples during the course of collecting the experimental PXRD data.[44]

The fundamental molecular unit of **1** is composed of a gigantic deca-La^{III} incorporated octameric selenotungstate $\{[W_{16}La_{10}(H_2O)_{38}O_{50}][B\text{-}\alpha\text{-}SeW_9O_{33}]_8\}^{38-}$ polyoxoanion (Figure 2a). In the octameric polyoxoanion, all the W^{VI} centers exhibit the octahedral coordination geometry with the W−O bond lengths of 1.671(18)−2.53(2) Å and the O−W−O angles of 68.6(7)−173.2(7)°. All the Se^{IV} heteroatoms display the triangular pyramidal coordination environment with the Se−O distances of 1.676(18)−1.751(16) Å and the O−Se−O angles of 95.4(8)−103.2(9)°. Attractively, the backbone structure of $\{[W_{16}La_{10}(H_2O)_{38}O_{50}][B\text{-}\alpha\text{-}SeW_9O_{33}]_8\}^{38-}$ can be considered that eight trivacant Keggin $[B\text{-}\alpha\text{-}SeW_9O_{33}]^{8-}$ segments occupy four vertices of a rectangle heterometallic cluster $[W_{16}La_{10}(H_2O)_{38}O_{50}]^{26+}$ with the size of about 9.94 × 16.53 Å (Figure 2b). Notably, all the $[B\text{-}\alpha\text{-}SeW_9O_{33}]^{8-}$ segments show

DOI: 10.1021/acs.cgd.7b00539
Cryst. Growth Des. 2017, 17, 3917−3928

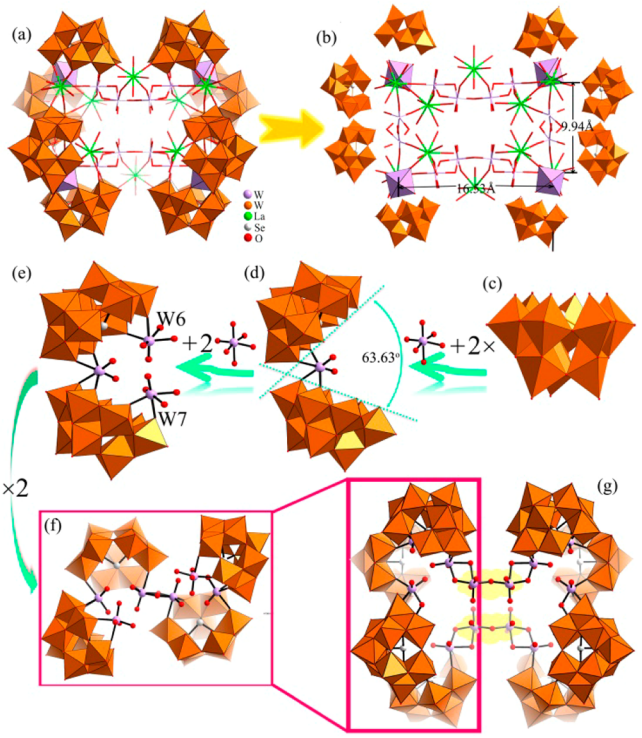

Figure 2. (a) Combined polyhedral and ball-and-stick view of the deca-La^{III} incorporated octameric selenotungstate polyoxoanion of **1**. (b) View of eight trivacant Keggin $[B\text{-}\alpha\text{-}SeW_9O_{33}]^{8-}$ segments occupying the four vertices of a rectangle heterometallic cluster $[W_{16}La_{10}(H_2O)_{38}O_{50}]^{26+}$. (c) Trivacant Keggin $[B\text{-}\alpha\text{-}SeW_9O_{33}]^{8-}$ unit in **1**. (d) $[Se_2W_{19}O_{68}]^{14-}$ unit in **1**. (e) $\{[W_3O_{10}][B\text{-}\alpha\text{-}SeW_9O_{33}]_2\}^{18-}$ segment in **1**. (f) Neoteric tetrameric $\{[W_6O_{18}][B\text{-}\alpha\text{-}SeW_9O_{33}]_4\}^{32-}$ cluster in **1**. (g) Occlusive octameric structure of $\{[W_{16}O_{50}][B\text{-}\alpha\text{-}SeW_9O_{33}]_8\}^{68-}$ in **1**.

the well-known trivacant α-Keggin-type structural feature, which can be thought of as a derivative of an edge-sharing $\{W_3O_{13}\}$ triad removing away from the hypothetical α-Keggin $[SeW_{12}O_{40}]^{4-}$ structure (Figure 2c). Intriguingly, in **1**, two $[B\text{-}\alpha\text{-}SeW_9O_{33}]^{8-}$ segments are linked to each other by sharing an extra $\{WO_6\}$ octahedron via four *cis* oxygen sites, leading to a dimeric $[Se_2W_{19}O_{68}]^{14-}$ segment with the "bite" angle of 63.63° (Figure 2d). Such $[Se_2W_{19}O_{68}]^{14-}$ group is fairly similar to the configuration of the $[As_2W_{19}O_{68}]^{16-}$ building block observed in $[H_2N(CH_3)_2]_8Na_8\{[W_3Eu_2(H_2O)_8AsO_8(OH)][B\text{-}\alpha\text{-}AsW_9O_{33}]_2\}_2\cdot 65H_2O$ reported by us[14] (Figure S4, Supporting Information). Compared with the $[As_2W_{19}O_{68}]^{16-}$ fragment, the "bite" angle (63.63°) of the $[Se_2W_{19}O_{68}]^{14-}$ segment in **1** is larger than that (63.02°) of the $[As_2W_{19}O_{68}]^{16-}$ segment, which may stem from the large radius of Se^{IV} center. Obviously, such lacunary fragment provides a nice opportunity to accommodate other metal centers. As shown in Figure 2e, two $\{WO_6\}$ octahedra bond with the exposed surface oxygen atoms in the "bite" angle of the $[Se_2W_{19}O_{68}]^{14-}$ segment to give a complicated $\{[W_3O_{10}][B\text{-}\alpha\text{-}SeW_9O_{33}]_2\}^{18-}$ segment. It should also be noted that two $\{[W_3O_{10}][B\text{-}\alpha\text{-}SeW_9O_{33}]_2\}^{18-}$ segments are further connected via the edge-sharing mode forming a neoteric tetrameric $\{[W_6O_{18}][B\text{-}\alpha\text{-}SeW_9O_{33}]_4\}^{32-}$ cluster (Figure 2f). Obviously, the spatial distribution of two $\{[W_3O_{10}][B\text{-}\alpha\text{-}SeW_9O_{33}]_2\}^{18-}$ segments in tetrameric $\{[W_6O_{18}][B\text{-}\alpha\text{-}SeW_9O_{33}]_4\}^{32-}$ cluster are in the staggered pattern, which is conducive to reduce the steric hindrance as much as possible (Figure S5, Supporting Information). Of particular interest is that two corner-sharing $[W_2O_{11}]^{10-}$ groups join two tetrameric $\{[W_6O_{18}][B\text{-}\alpha\text{-}SeW_9O_{33}]_4\}^{32-}$ clusters generating an unseen occlusive octameric structure $\{[W_{16}O_{50}][B\text{-}\alpha\text{-}SeW_9O_{33}]_8\}^{68-}$ (Figure 2g). As a matter of fact, such occlusive octameric selenotungstate cluster $\{[W_{16}O_{50}][B\text{-}\alpha\text{-}SeW_9O_{33}]_8\}^{68-}$ is stabilized by ten extraneous La^{III} ions in the structure of **1**. From the viewpoint of crystallography, these exist five crystallographically independent La^{III} ions ($La1^{III}$, $La2^{III}$, $La3^{III}$, $La4^{III}$, $La5^{III}$) in the fundamental molecular unit of **1** (Figures 3a,c,d), which all display the distorted monocapped square antiprism geometry (Figure S6, Supporting Information). $La1^{III}$ and $La5^{III}$ cations have the similar coordination environments, while $La2^{III}$ and $La3^{III}$ cations have the similar coordination environments; as a

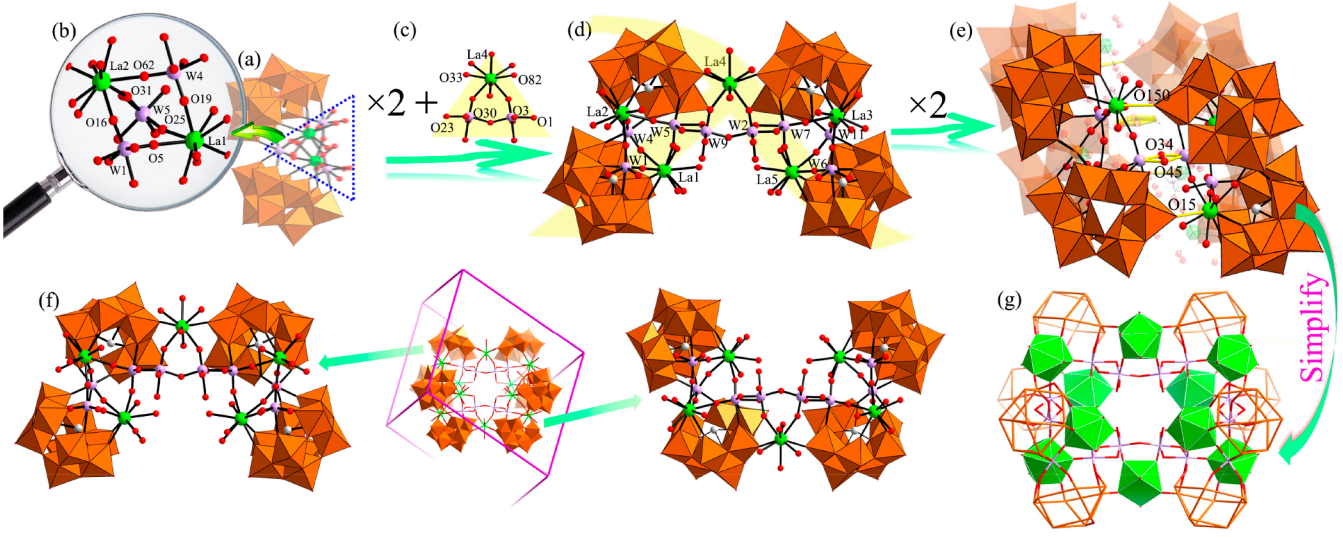

Figure 3. (a) View of the $\{[W_3O_{11}La_2(H_2O)_7][B\text{-}\alpha\text{-}SeW_9O_{33}]_2\}^{14-}$ segment in **1**. (b) Magnifying view of the connection mode of two embedded La^{3+} ions. (c) View of the $[W_2O_{13}La(H_2O)_5]^{11-}$ segment. (d) View of the λ-shaped $\{[W_8O_{29}La_5(H_2O)_{19}][B\text{-}\alpha\text{-}SeW_9O_{33}]_4\}^{27-}$ subunit. (e) View of the deca-La^{III}-embedded cluster $\{[W_{16}La_{10}(H_2O)_{38}O_{50}][B\text{-}\alpha\text{-}SeW_9O_{33}]_8\}^{38-}$ in **1**. (f) Reverse arrangement of two $\{[W_8O_{29}La_5(H_2O)_{19}][B\text{-}\alpha\text{-}SeW_9O_{33}]_4\}^{27-}$ fragments in **1**. (g) Simplified view of the structure of **1**.

DOI: 10.1021/acs.cgd.7b00539
Cryst. Growth Des. 2017, 17, 3917−3928

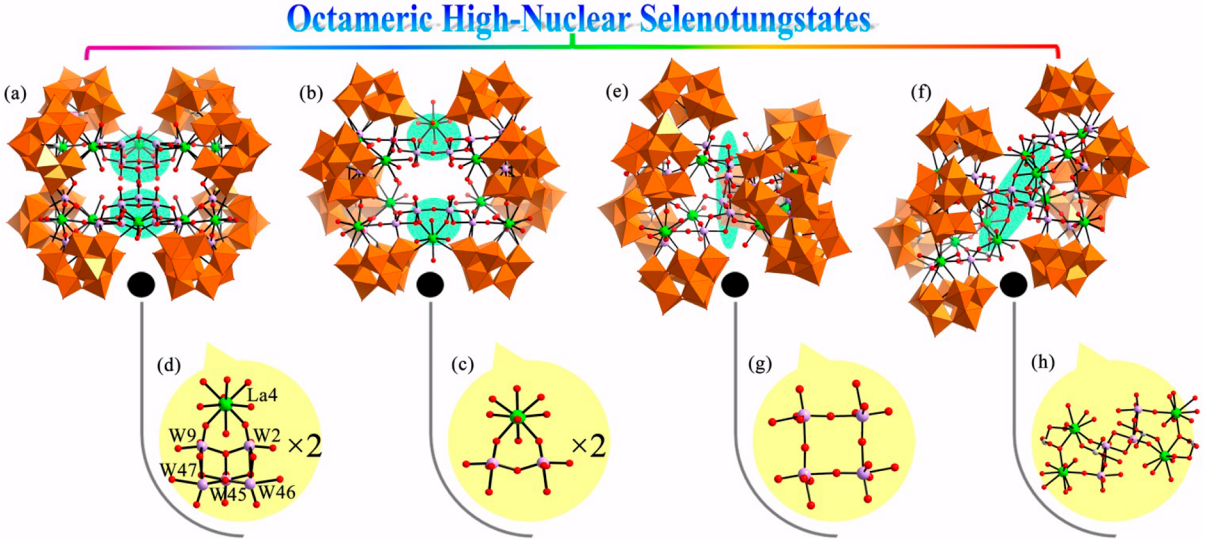

Figure 4. (a) View of the molecular structural unit of **3**. (b) View of the molecular structural unit of **1**. (c) View of the $[W_2O_{13}La(H_2O)_5]^{11-}$ segment in **1**. (d) View of the $[W_3O_{18}La(H_2O)_5]^{15-}$ segment in **3**. (e) View of the molecular structural unit of $[\{(SeO_3)W_{10}O_{34}\}_8\{Ce_8(H_2O)_{20}\}(WO_2)_4(W_4O_{12})]^{48-}$ (**a**). (f) View of the molecular structural unit of $[\{(SeO_3)W_{10}O_{34}\}_8\{Ce_8(H_2O)_{20}\}(WO_2)_4\{(W_4O_6)Ce_4(H_2O)_{14}(SeO_3)_4(NO_3)_2\}]^{34-}$ (**b**). (g) View of the $[W_4O_{20}]^{16-}$ segment in **a**. (h) View of the $[(W_4O_6)Ce_4(H_2O)_{14}(NO_3)_2(SeO_3)_4]^{14+}$ segment in **b**.

result, only $La1^{III}$, $La2^{III}$ and $La4^{III}$ are described here. It can be clearly seen that the nine-coordinate $La1^{III}$ and $La2^{III}$ cations are encapsulated in the $\{[W_3O_{10}][B\text{-}\alpha\text{-}SeW_9O_{33}]_2\}^{18-}$ segment and combined with each other via three La−O−W−O−La bonds (La2−O62−W4−O19−La1, La2−O31−W5−O25−La1, La2−O16−W1−O5−La1), creating the asymmetrical sandwich-type $\{[W_3O_{11}La_2(H_2O)_7][B\text{-}\alpha\text{-}SeW_9O_{33}]_2\}^{14-}$ segment (Figures 3a,b). The coordination geometry of the $La1^{III}$ cation is established by five oxygen atoms from the $\{[W_3O_{10}][B\text{-}\alpha\text{-}SeW_9O_{33}]_2\}^{18-}$ unit [La1−O: 2.447(15)−2.505(17) Å] and four coordinate water molecules [La1−O: 2.51(2)−2.75(2) Å] (Figure S6a, Supporting Information). The coordination sphere of the $La2^{III}$ cation is completed by five μ_2-O atoms from five $\{WO_6\}$ octahedra in the central belt of $\{[W_3O_{10}][B\text{-}\alpha\text{-}SeW_9O_{33}]_2\}^{18-}$ fragment [La2−O: 2.456(17)−2.535(17) Å], one μ_2-O atoms from another $\{[W_3O_{11}La_2(H_2O)_7][B\text{-}\alpha\text{-}SeW_9O_{33}]_2\}^{14-}$ fragment [La2−O150: 2.778(17) Å], and three water ligands [La2−O: 2.50(2)−2.563(18) Å] (Figure S6b, Supporting Information). Based on the above-mentioned connection mode, the dimeric sandwich-type $\{[W_3O_{11}La_2(H_2O)_7][B\text{-}\alpha\text{-}SeW_9O_{33}]_2\}^{14-}$ segment can be regarded as two trivacant $[B\text{-}\alpha\text{-}SeW_9O_{33}]^{8-}$ subunits sandwiching a $[W_3La_2O_{23}(H_2O)_7]^{2+}$ core or a divacant $\{[W_3O_{10}][B\text{-}\alpha\text{-}SeW_9O_{33}]_2\}^{18-}$ fragment encapsulating two La^{III} cations.[45] With regard to $La4^{III}$ cation, it is chelated by two O atoms provided by two $[B\text{-}\alpha\text{-}SeW_9O_{33}]^{8-}$ subunits [La4−O33: 2.514(18) Å, La4−O82: 2.522(18) Å], two O atoms from the bridging $[W_2O_{11}]^{10-}$ group [La4−O56: 2.499(17) Å, La4−O88:2.533(17) Å] and five water molecules [La4−O: 2.513(18)−2.65(2) Å] (Figure 3d and Figure S6c, Supporting Information). Alternatively, the $\{[W_{16}La_{10}(H_2O)_{38}O_{50}][B\text{-}\alpha\text{-}SeW_9O_{33}]_8\}^{38-}$ cluster anion in **1** can be viewed as the assembly of four $\{[W_3O_{11}La_2(H_2O)_7][B\text{-}\alpha\text{-}SeW_9O_{33}]_2\}^{14-}$ units. First, the bridging $[LaW_2O_{13}(H_2O)_5]^{11-}$ segment (Figure 3c) joins two $\{[W_3O_{11}La_2(H_2O)_7][B\text{-}\alpha\text{-}SeW_9O_{33}]_2\}^{14-}$ fragments and creates a λ-shaped $\{[W_8O_{29}La_5(H_2O)_{19}][B\text{-}\alpha\text{-}SeW_9O_{33}]_4\}^{27-}$ architecture (Figure 3d). Then, the identical $\{[W_8O_{29}La_5(H_2O)_{19}][B\text{-}\alpha\text{-}SeW_9O_{33}]_4\}^{27-}$ moieties are related to each other by a 180° rotation, giving a ten-La^{III}-embedded octameric $\{[W_{16}La_{10}(H_2O)_{38}O_{50}][B\text{-}\alpha\text{-}SeW_9O_{33}]_8\}^{38-}$ cluster anion of **1** (Figure 3e). Moreover, the bridging mode between two $\{[W_8O_{29}La_5(H_2O)_{19}][B\text{-}\alpha\text{-}SeW_9O_{33}]_4\}^{27-}$ fragments shows that each $\{[W_3O_{11}La_2(H_2O)_7][B\text{-}\alpha\text{-}SeW_9O_{33}]_2\}^{14-}$ unit in the tetramer $\{[W_8O_{29}La_5(H_2O)_{19}][B\text{-}\alpha\text{-}SeW_9O_{33}]_4\}^{27-}$ provides four nodes to link another $\{[W_3O_{11}La_2(H_2O)_7][B\text{-}\alpha\text{-}SeW_9O_{33}]_2\}^{14-}$ unit (namely, O150, O34, O45, and O15), forming a rectangular-like arrangement (Figure 3e; Figure S7, Supporting Information). There is no doubt that the ten encapsulated La^{III} ions make a significant contribution in stabilizing the whole $\{[W_{16}La_{10}(H_2O)_{38}O_{50}][B\text{-}\alpha\text{-}SeW_9O_{33}]_8\}^{38-}$ cluster anion of **1**, which may also indicating the great potential in constructing the large-sized high-nuclear LEHPOMs by the synergistic effect of lone-electron-pair containing selenotungstate fragments and Ln cations (Figure 3g).

The molecular unit of **3** includes a centrosymmetric octameric $\{[W_{18}La_{10}(H_2O)_{34}O_{56}][B\text{-}\alpha\text{-}SeW_9O_{33}]_8\}^{38-}$ polyoxoanion (Figure 4a). The polyoxoanionic skeleton of **3** is very analogous to **1** except the number of bridging W^{VI} centers. Upon a close inspection, it can be found that **1** is established by two $\{[W_6La_4(H_2O)_{14}O_{18}][B\text{-}\alpha\text{-}SeW_9O_{33}]_4\}^{20-}$ tetrameric subunits and two bridging triangular $[W_2O_{13}La(H_2O)_5]^{11-}$ groups (Figures 4b,c), whereas the connective groups between two tetrameric $\{[W_6La_4(H_2O)_{14}O_{18}][B\text{-}\alpha\text{-}SeW_9O_{33}]_4\}^{20-}$ subunits in **3** are two novel $[W_3O_{18}La(H_2O)_5]^{15-}$ segments (Figure 4d). Notably, the site occupancies of W45, W46, and W47 in $[W_3O_{18}La(H_2O)_5]^{15-}$ segment are 50%, 25%, and 25%, respectively (Figure S8, Supporting Information). Similarly, after removing all the La^{III} ions, there still exist an occlusive octameric polyoxotungstate framework in **3** constructed from eight $[B\text{-}\alpha\text{-}SeW_9O_{33}]^{8-}$ units and 18 bridging W^{VI} centers (Figure S9, Supporting Information).

Hitherto, analogous octameric high-nuclear selenotungstates are rare, and only two Ln-stabilized octameric selenotungstates $[\{(SeO_3)W_{10}O_{34}\}_8\{Ce_8(H_2O)_{20}\}(WO_2)_4(W_4O_{12})]^{48-}$ (**a**) (Figure 4e) and $[\{(SeO_3)W_{10}O_{34}\}_8\{Ce_8(H_2O)_{20}\}(WO_2)_4\{(W_4O_6)Ce_4(H_2O)_{14}(SeO_3)_4(NO_3)_2\}]^{34-}$ (**b**) (Figure 4f) have been isolated so far.[25] Comparing **1**−**4** with **a**−**b**, two common features are observed showing that they are all obtained by the

DOI: 10.1021/acs.cgd.7b00539
Cryst. Growth Des. 2017, 17, 3917−3928

one-step self-assembly strategy and contain four asymmetrical sandwich-type $\{[W_3O_mLn_2(H_2O)_n][B\text{-}\alpha\text{-}SeW_9O_{33}]_2\}^{x-}$ units and additional $\{WO_6\}$ octahedra. Their main differences are also observed. The connection modes between two tetrameric subunits in **a** and **b** are the planar $[W_4O_{20}]^{16-}$ group (Figure 4g) and the novel $[(W_4O_6)Ce_4(H_2O)_{14}(NO_3)_2(SeO_3)_4]^{14+}$ group (Figure 4h), respectively. With regard to **1**−**4**, two $[W_2O_{13}La(H_2O)_5]^{11-}$ segments (Figure 4c) and two $[W_3O_{18}La(H_2O)_5]^{15-}$ segments (Figure 4d) are respectively captured by two tetrameric subunits and then joined them together to construct the final octameric structures.

The molecular structural unit of **5** is composed of an octameric $[W_{16}Nd_{10}O_{50}(H_2O)_{34}(B\text{-}\alpha\text{-}AsW_9O_{33})_8]^{46-}$ polyoxoanion (Figure 5a), a bridging $[Nd(H_2O)_7]^{3+}$ cation, four Na^+ cations, 21 protons, 18 $[H_2N(CH_3)_2]^+$ cations, and 60 lattice water molecules. In comparison to **1**, the main polyoxoanionic backbone of **5** remains unchanged with slight differences in coordination environments for the embedded Ln^{III} anions. In the half unit of the polyoxoanion $[W_{16}Nd_{10}O_{50}(H_2O)_{34}(B\text{-}\alpha\text{-}AsW_9O_{33})_8]^{46-}$ in **5**, the $Nd2^{III}$, $Nd3^{III}$, $Nd4^{III}$, and $Nd6^{III}$ exhibit the eight-coordinate distorted square antiprismatic geometries, which are all defined by five μ_2-oxygen atoms from the $\{[W_3Nd_2(H_2O)_6O_{10}][B\text{-}\alpha\text{-}AsW_9O_{33}]_2\}^{14-}$ units [Nd−O: 2.334(14)−2.489(14) Å] and three μ_2-oxygen atoms from water molecules [Nd−O: 2.486(17)−2.563(15) Å] (Figure S10, Supporting Information). In terms of $La1^{III}$ and $La2^{III}$ ions in the $\{[W_3O_{11}La_2(H_2O)_7][B\text{-}\alpha\text{-}SeW_9O_{33}]_2\}^{14-}$ fragment of **1**, their coordination environments are different although they have the same monocapped square antiprism geometries. Hence, only the dimeric $\{[W_3Nd_2(H_2O)_6O_{10}][B\text{-}\alpha\text{-}AsW_9O_{33}]_2\}^{14-}$ units (Figure 5b) in **5** can be considered as a fusion of two half-units $[AsW_{11}O_{42}Nd(H_2O)_3]^{12-}$ by sharing a $\{WO_6\}$ octahedron (Figure 5c). Additionally, due to the different coordination environments of Ln^{III} ions in **1** and **5**, the bridging modes between the two λ-shaped tetramers are also different. In **5**, the connection motif between two adjacent $\{[W_8Nd_5O_{27}(H_2O)_{17}][B\text{-}\alpha\text{-}AsW_9O_{33}]_4\}^{27-}$ subunits is only through four W−O−W bridges (W1A−O83A−W3A, W1A−O44A−W3A, W3−O44−W1, W3−O83−W1) (Figure 5d). Nevertheless, two $\{[W_8O_{29}La_5(H_2O)_{19}][B\text{-}\alpha\text{-}SeW_9O_{33}]_4\}^{27-}$ units in **1** are linked to each other through La−O−W bridges and W−O−W bridges forming a rectangular connection mode (Figure 3e; Figure S7, Supporting Information). Strikingly, **5** reveals an unprecedented 1-D chain-like alignment based on $\{[W_{16}Nd_{10}(H_2O)_{34}O_{50}][B\text{-}\alpha\text{-}AsW_9O_{33}]_8\}^{46-}$ polyoxoanions and Nd^{3+} bridges (Figure 5e). The coordination sphere of the Nd^{III} connector is completed by two terminal oxygen atoms from two neighboring $\{[W_3O_{10}Nd_2(H_2O)_6][B\text{-}\alpha\text{-}AsW_9O_{33}]_2\}^{14-}$ anions [Nd5−O53: 2.450(19) Å. Nd5−O129: 2.419(17) Å] and seven water ligands [Nd5−O: 2.44(4)−2.75(4) Å], exhibiting a monocapped square antiprismatic geometry (Figure S10e, Supporting Information). For all we know, **5** represents the first example of the 1-D chain-like arsenotungstate built by $\{[W_{16}Nd_{10}(H_2O)_{34}O_{50}][B\text{-}\alpha\text{-}AsW_9O_{33}]_8\}^{46-}$ polyoxoanions and Nd^{III} bridges. In comparison with the Yb_{10}-encapsulated complex $[Yb_{10}As_{10}W_{88}O_{308}(OH)_8(H_2O)_{28}(OAc)_4]^{40-}$ (**c**) reported by Boskovic's group (Figure S11, Supporting Information),[21] some obvious differences between **5** and **c** can be recited on three aspects: (i) **5** was synthesized by reaction of Na_2WO_4 and $NaAsO_2$ with $Nd(NO_3)_3{\cdot}6H_2O$ at pH 4.0, whereas **c** was prepared by reacting $Na_9[B\text{-}\alpha\text{-}AsW_9O_{33}]$ with $YbCl_3{\cdot}3H_2O$ in a 1:3 molar ratio in the NaOAc−AcOH buffer at pH 4.7; (ii) After the removal of the Ln^{III} ions, the octameric structure in **5** can still be retained. On the contrary, two asymmetric units in **c** are linked through two Yb^{III} ions; hence, the octameric structure will be split into two identical parts when the Yb^{III} ions are removed; (iii) **5** is a 1-D chain-like structure, whereas **c** is merely a discrete structure.

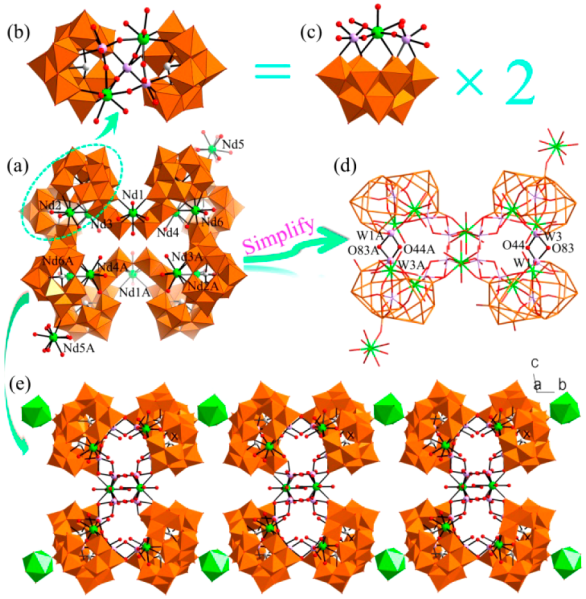

Figure 5. (a) Combined polyhedral and ball-and-stick view of the molecular structural unit of **5**. The atoms with A in their labels are symmetrically generated (A: $-x$, $2-y$, $-z$). (b) View of the $\{[W_3O_{10}La_2(H_2O)_6][B\text{-}\alpha\text{-}AsW_9O_{33}]_2\}^{14-}$ unit. (c) $[AsW_{11}O_{42}Nd(H_2O)_3]^{12-}$ segment. (d) Simplified drawing highlighting four W−O−W bridges between two $\{[W_8Nd_5O_{27}(H_2O)_{17}][B\text{-}\alpha\text{-}AsW_9O_{33}]_4\}^{27-}$ units. (e) One-dimensional chain-like structure of **5** along the *b* axis.

IR Spectra. IR spectra for solid-state samples **1**−**5** were recorded in the range of 4000 and 400 cm^{-1} with KBr pellets on a Nicolet 170 SXFT−IR spectrometer (Figure S1, Supporting Information). Their IR spectra display four characteristic vibration patterns derived from the lacunary Keggin POM framework in 1000−650 cm^{-1}. Four characteristic vibration bands attributed to $\nu_{as}(W{-}O_t)$, $\nu_{as}(X{-}O_a)$ (X = Se^{IV}, As^{III}), $\nu_{as}(W{-}O_b)$, and $\nu_{as}(W{-}O_c)$, respectively, appear at 970, 873, 790, and 735 cm^{-1} for **1**, 971, 873, 787, and 735 cm^{-1} for **2**, 971, 873, 789, and 738 cm^{-1} for **3**, 970, 873, 790, and 738 cm^{-1} for **4**, and 952, 873, 784, and 716 cm^{-1} for **5**. Notably, the resemblance of IR spectra of **1**−**5** in the low-wavenumber domain indicates that all of them contain the trivacant $[B\text{-}\alpha\text{-}XW_9O_{33}]^{n-}$ (X = Se^{IV}, As^{III}) units. In the high-frequency region, the intense and broad absorption bands at 3428−3439 cm^{-1} are observed, corresponding to the stretching mode of the coordinate and lattice water molecules. In addition, the N−H and C−H stretching vibrations appear at 3155−3168 and 2796−2801 cm^{-1}, while the N−H and C−H bending vibration bands can be observed at 1621−1522 and 1493−1461 cm^{-1}. The occurrence of these signals confirms the existence of dimethylamine groups. Compared with the IR spectrum of dimethylamine hydrochloride, the N−H vibration bands in **1**−**5** have the noticeable hypochromatic shifts, suggesting the presence of electrostatic interactions and hydrogen-bonding interactions. Furthermore, there is no appearance of the Ln−O stretching vibration in the IR region, which may result from the predominant ionic interactions between Ln^{III} cations and vacant polyoxotungstate units. In a

DOI: 10.1021/acs.cgd.7b00539
Cryst. Growth Des. 2017, 17, 3917−3928

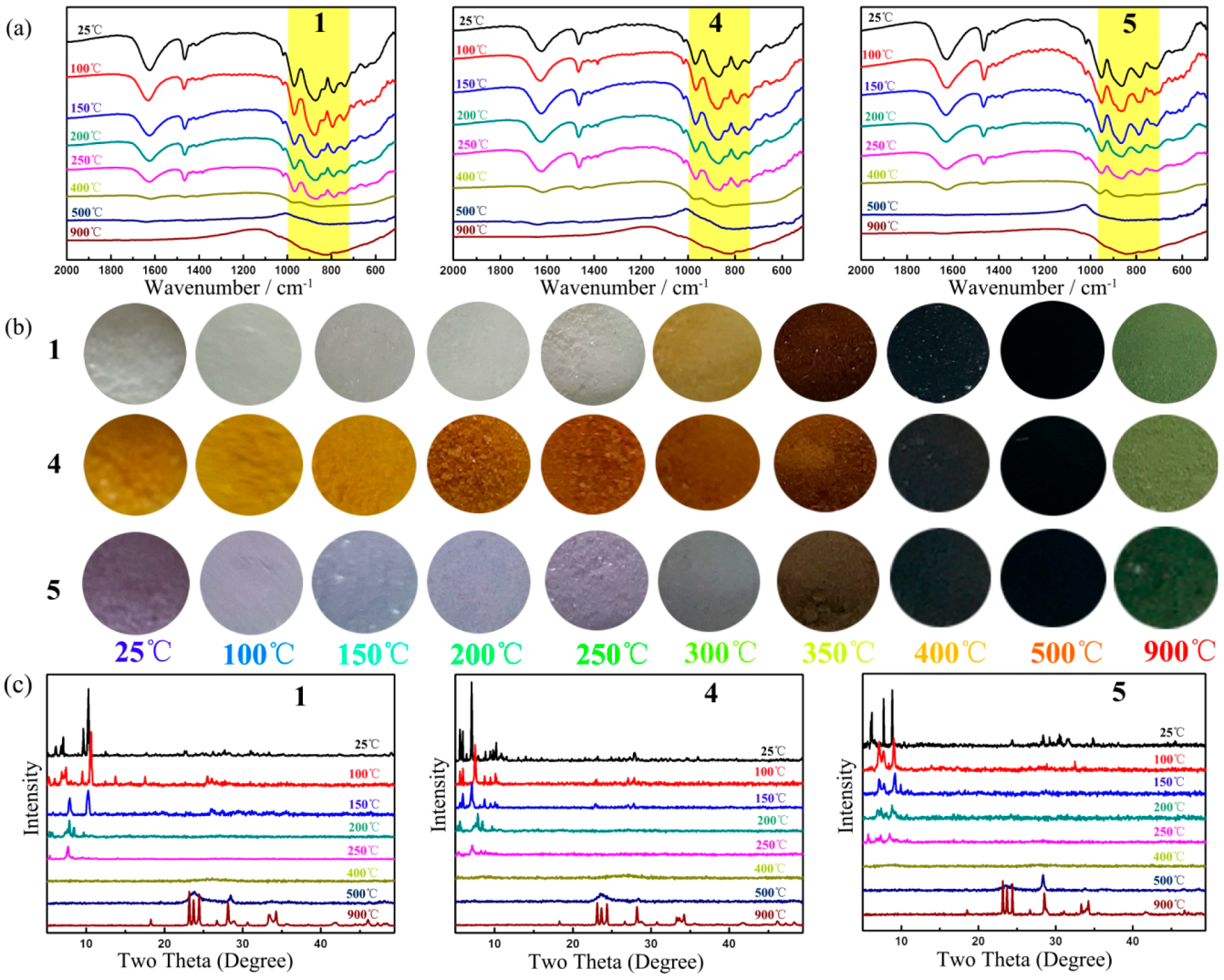

Figure 6. (a) Variable-temperature IR spectra for **1**, **4**, and **5**. (b) Coloration changes of **1**, **4**, and **5** at different temperatures. (c) Variable-temperature PXRD patterns for **1**, **4**, and **5**.

word, the results of IR spectra are in good agreement with those from the single-crystal structural analyses.

TG Analyses. To investigate the thermal stability of **1**−**5**, the TG analyses were carried out under N_2 atmosphere from 25 to 1000 °C at a heating rate of 10 °C min^{-1} (Figure S12, Supporting Information). The TG curves reveal that the weight loss processes of all the compounds can be divided into two steps. In the case of **1**−**2**, the first weight loss of 6.49% (calcd. 6.23%) for **1** and 6.25% (calcd. 6.23%) for **2** are from 25 to 200 °C, which corresponds to the liberation of 56 lattice water molecules and 34 coordinate water molecules. The second weight loss of 7.49% (calcd. 7.36%) for **1** and 7.19% (calcd. 7.36%) for **2** from 200 to 1000 °C are attributable to the dehydration of 36 protons and the removal of four coordinate water molecules and 16 dimethylamine molecules, and the sublimation of eight SeO_2 molecules stemming from the decomposition of polyoxoanion. As for **3**−**4**, the first weight loss of 6.27% (calcd. 6.50%) for **3** and 6.49% (calcd. 6.50%) for **4** occurring from 25 to 200 °C corresponds to the loss of 80 lattice water molecules and 17 coordinate water molecules. Then, upon further heating, the second weight loss 9.27% (calcd. 9.30%) for **3** and 8.60% (calcd. 9.27%) for **4** between 200 to 1000 °C involves the dehydration of 34 protons, the loss of 17 coordinate water molecules and 22 dimethylamine molecules, and the sublimation of eight SeO_2 molecules originating from the decomposition of polyoxoanion. With respect to **5**, the weight loss from 25 to 200 °C is 6.48% (calcd. 6.49%), corresponding to the departure of 60 lattice water molecules and 34 coordinate water molecules. Then, the second weight loss of 7.96% (calcd. 7.96%) between 200 to 1000 °C involves the dehydration of 39 protons, the liberation of seven coordinate water molecules and 18 dimethylamine molecules, and the release of four As_2O_3 molecules resulting from the decomposition of polyoxoanion.

In order to further understand the details in the process of thermolysis, the variable-temperature IR spectra, coloration changes as well as the variable-temperature PXRD patterns at different temperatures for **1**, **4**, and **5** have been collected (Figure 6). As can be seen from variable-temperature IR spectra, there are no shifts for the four asymmetric stretching vibrations $\nu_{as}(W-O_t)$, $\nu_{as}(X-O_a)$ ($X = Se^{IV}$, As^{III}), $\nu_{as}(W-O_b)$, and $\nu_{as}(W-O_t)$ from 25 to 250 °C, indicating that the skeletons of POMs are unchanged aside from the removal of lattice and coordinate water molecules. While, from 250 to 500 °C, the characteristic vibration bands of POMs in low-wavelength region gradually disappear, the absorption strength for the $\nu(N-H)$ and $\nu(C-H)$ vibration bands are weakened (Figure 6a). That is to say, the

DOI: 10.1021/acs.cgd.7b00539
Cryst. Growth Des. 2017, 17, 3917−3928

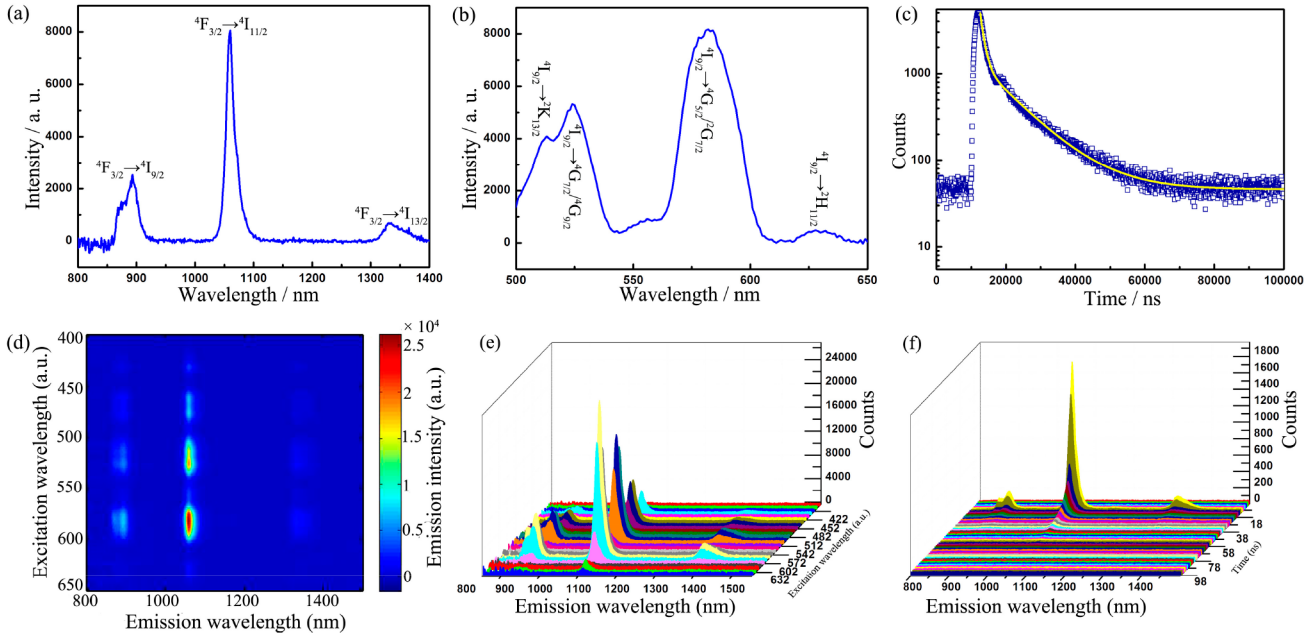

Figure 7. (a) Emission spectrum of **5** under excitation at 582 nm. (b) Excitation spectrum of **5** obtained by monitoring the emission at 1060 nm. (c) Decay curves of **5** monitored under the excitation at 582 nm and the emissions at 1060 nm. (d) Luminescence photoexcitation maps. Contour plots of the photoluminescence emission intensity as a function of emission and excitation wavelengths for **5**. (e) Three-dimensional diagram of the luminescence photoexcitation maps. (f) Time-resolved fluorescence spectrum at different emission wavelengths of **5**.

thermal decomposition of POM skeleton is occurring. What's more, in this heating process, the colors for **1**, **4**, and **5** become dark gradually and display the black at 500 °C, which is derived from the carbonization of dimethylamine ingredient (Figure 6b).[46] As the temperature rises to 900 °C, the ν(N−H) and ν(C−H) vibration bands in IR spectra completely disappear and the black colors of samples fade, which indicate the removal of all the dimethylamine components (Figure 6b). Furthermore, the variable-temperature PXRD patterns of **1**, **4**, and **5** can further demonstrate the results of TG analyses and variable-temperature IR spectra. As shown in Figure 6c, the characteristic peaks in the corresponding PXRD patterns at the low 2θ angles can be still kept when the samples are heated to 250 °C, indicating that their polyoxoanionic skeletons are maintained. As a rule, the removal of lattice water and coordinate water molecules will make the crystalline samples effloresce. Thus, there are some differences at the low 2θ angles and the weakness of some peaks at the high 2θ angles of PXRD patterns between 25 to 250 °C. Nevertheless, from 250 to 900 °C, the peaks in PXRD patterns appearing at 6.8°−11.2° begin to decrease gradually and several new peaks located at 22.5°−35.0° turn up, implying the gradual decomposition of the main polyoxoanionic framework (Figure 6c). In order to find out the whereabouts of Ln elements, the PXRD spectra of corresponding lanthanide oxides (Ln_2O_3) were performed (Figure S13, Supporting Information). Compared with the PXRD spectra of the final mixed phases, the peaks of corresponding Ln_2O_3 are included in the spectra of the final mixed phases, implying that the Ln elements exist in the form of oxides in the residuals at 900 °C. All in all, the results of the variable-temperature IR spectra, coloration changes, and the variable-temperature PXRD patterns coincide with the TG analyses.

Photoluminescence Properties. In early time, the photoluminescence spectra for Tb^{III}- or Eu^{III}-containing compounds have been widely studied due to their intense line-like emission in UV−visible region, which can be known from a large number of literatures. Conversely, for the near-infrared (NIR) Ln emitters Pr^{III}, Nd^{III}, Sm^{III}, Dy^{III}, Ho^{III}, Er^{III}, and Yb^{III}, their photophysical properties have been comparatively less investigated.[47] Nevertheless, recently, increasing interest in NIR Ln emitters has been attracted resulting from their possible applications in telecommunication, biomedical, and photonic fields.[48−50] Hence, the solid state luminescence properties of **5** have been investigated at room temperature. The NIR luminescence spectrum of **5** has been collected under the excitation at 582 nm and exhibits three characteristic emission peaks of Nd^{III} ions at 893 nm ($^4F_{3/2}\rightarrow{}^4I_{9/2}$), 1060 nm ($^4F_{3/2}\rightarrow{}^4I_{11/2}$), and 1331 nm ($^4F_{3/2}\rightarrow{}^4I_{13/2}$) (Figure 7a). The excitation spectrum obtained by monitoring the most emission band ($^4F_{3/2}\rightarrow{}^4I_{11/2}$) at 1060 nm displays four peaks at 513, 524, 582, and 628 nm, which are respectively attributed to the $^4I_{9/2}\rightarrow{}^2K_{13/2}$, $^4I_{9/2}\rightarrow{}^4G_{7/2}/^4G_{9/2}$, $^4I_{9/2}\rightarrow{}^4G_{5/2}/^2G_{7/2}$, and $^4I_{9/2}\rightarrow{}^2H_{11/2}$ transitions (Figure 7b).[51−53] As we know, the luminescence decay measurement is an exceptionally helpful tool for investigating the dynamics of excited states.[54] In order to determine the lifetime, the solid-state luminescence decay curve of **5** has been measured under the excitation at 582 nm and the most intense emission at 1060 nm ($^4F_{3/2}\rightarrow{}^4I_{11/2}$) (Figure 7c). The decay curve can be well- fitted with a second-order exponential function of $I = A_1\exp(-t/\tau_1) + A_2\exp(-t/\tau_2)$ (where I is the luminescence intensity, t is the time; A_1 and A_2 are the pre-exponential factors; and τ_1 and τ_2 are the fast and slow components of the luminescence lifetimes), affording the luminescence lifetimes τ_1 and τ_2 of 1.11 μs (24.97%) and 10.55 μs (75.03%) and pre-exponential factors A_1 and A_2 of 3872.94 and 1220.78. As a result, the average decay time (τ^*) can be determined using the following equation: $\tau^* = (A_1\tau_1^2 + A_2\tau_2^2)/(A_1\tau_1 + A_2\tau_2)$.[55] Thus, the average lifetime is calculated to be 8.17 μs. Moreover, we have also investigated the excitation wavelength-dependent photoluminescence emission spectra of **5** to gain more details about the emission behavior (Figures 7d,e). Clearly, there is no obvious shift for the most intense emission band in the resulting luminescence spectra

DOI: 10.1021/acs.cgd.7b00539
Cryst. Growth Des. 2017, 17, 3917−3928

when the emission wavelength varies from 422 to 632 nm. Compared with the multiemission behavior, this phenomenon in **5** may be related to the same emission state ($^4F_{3/2}$) of three electron transition processes.[56] However, their emission intensities are found to be dependent on the excitation wavelengths. When the excitation wavelength is tuned to 582 nm, the emission spectrum exhibits the maximum intensity, which is very helpful for us to verify the best excitation wavelength. As we know, in the UV−visible region, the intramolecular energy transfer of the oxygen-to-metal (O → W) charge-transfer transitions can sensitize the emission of Ln cations in the reported LEHPOMs.[31,57] To figure out whether the energy transfer between the Nd^{3+} ions and the arsenotungstate fragments in **5** occurs in the NIR region, the time-resolved luminescence measurements were performed. As shown in Figure 7f, the relative proportions of the emission intensities of three characteristic emission bands of Nd^{3+} ions keep notably unchanged with increasing the decay time and the emission spectral shape remain prominently unchanged. This observation indicates no occurrence of the intramolecular energy transfer of the oxygen-to-metal (O → W) charge-transfer transitions sensitizing the emission of Nd^{III} cations in **5** in the NIR region. In order to further confirm this case, the NIR emission spectrum of $K_{14}[As_2W_{19}O_{67}(H_2O)]$ has been also collected under the same measurement conditions to **5**, in which no emission band is seen (Figure S14, Supporting Information). This result indeed verifies the absence of the oxygen-to-metal (O → W) charge-transfer transitions sensitizing the emission of Nd^{3+} cations in **5**. That is, arsenotungstate fragments in **5** do not make a contribution in the luminescence process. As a result, two different luminescence lifetimes τ_1 and τ_2 of 1.11 μs (24.97%) and 10.55 μs (75.03%) derived from the fitting of second-order exponential function mainly result from the Nd^{III} cations. According to the structural discussion of **5**, there are two types of coordination geometries of six crystallographically independent Nd^{3+} cations in the structure of **5** and Nd2, Nd3, Nd4, and Nd6 cations inhabit in the eight-coordinate square antiprism geometry with three coordinate water molecules, while the Nd1 and Nd6 cations resides in the nine-coordinate monocappped square antiprism geometry with five or seven coordinate water molecules. It is well-known that high frequency O−H oscillators in water ligands usually quench the luminescence emission.[40,58,59] Thus, it can be speculated that the fast component (τ_1) of the luminescence lifetime majorly may originate from the nine-coordinate monocappped square antiprism geometry, whereas the slow component (τ_2) of the luminescence lifetime principally may stem from the eight-coordinate square antiprism geometry.

CONCLUSIONS

In conclusion, five protonated dimethylamine balanced HNLEHPOMs $[H_2N(CH_3)_2]_{16}Na_9LnH_{10}\{[W_{16}Ln_{10}(H_2O)_{38}O_{50}][B\text{-}\alpha\text{-}SeW_9O_{33}]_8\}\cdot 56H_2O$ [Ln = La^{III} (**1**), Ce^{III} (**2**)], $[H_2N(CH_3)_2]_{22}Na_4H_{12}\{[W_{18}Ln_{10}(H_2O)_{34}O_{56}][B\text{-}\alpha\text{-}SeW_9O_{33}]_8\}\cdot 80H_2O$ [Ln = La^{III} (**3**), Ce^{III} (**4**)], and $Na_4[H_2N(CH_3)_2]_{18}H_{21}[Nd(H_2O)_7][W_{16}Nd_{10}O_{50}(H_2O)_{34}(B\text{-}\alpha\text{-}AsW_9O_{33})_8]\cdot 69H_2O$ (**5**) were synthesized in aqueous solution via the one-step self-assembly reaction of simple starting materials and structurally characterized. Remarkably, all of them contain eight $[B\text{-}\alpha\text{-}XW_9O_{33}]^{n-}$ (X = Se^{IV}, As^{III}) units connecting to each other by addition of $\{WO_6\}$ groups and Ln centers. Discriminatively, there are 16 bridging $\{WO_6\}$ octahedra in isostructural **1**−**2** and 18 bridging $\{WO_6\}$ octahedra in isostructural **3**−**4**. As for **5**, the most remarkable characteristic is that it shows the first 1-D chain-like architecture made up of $\{[W_{16}Nd_{10}(H_2O)_{34}O_{50}][B\text{-}\alpha\text{-}AsW_9O_{33}]_8\}^{46-}$ polyoxoanions and Nd^{III} bridges. Furthermore, the magnetic properties, luminescence properties, and thermostability analysis combined with the variable-temperature PXRD spectra and variable-temperature IR spectra have been also investigated. This work further confirms that DMAHC is an effective solubilizing agent in the preparation of HNLEHPOMs and that the pH-controlled utilization can tune the structural diversity of HNLEHPOM assemblies, which gives us the useful guidance in continuously exploring and creating novel organic−inorganic hybrid HNLEHPOMs by virtue of the appropriate choice of other organo-counterions, organic ligands, and reaction conditions.

ASSOCIATED CONTENT

Supporting Information

The Supporting Information is available free of charge on the ACS Publications website at DOI: 10.1021/acs.cgd.7b00539.

Crystal data of **1**−**5** (PDF)

IR spectra, additional structural figures, magnetic discussion, UV spectra, and TG curves (PDF)

Accession Codes

CCDC 1544228−1544232 contain the supplementary crystallographic data for this paper. These data can be obtained free of charge via www.ccdc.cam.ac.uk/data_request/cif, or by emailing data_request@ccdc.cam.ac.uk, or by contacting The Cambridge Crystallographic Data Centre, 12 Union Road, Cambridge CB2 1EZ, UK; fax: +44 1223 336033.

AUTHOR INFORMATION

Corresponding Authors

*E-mail: ljchen@henu.edu.cn.

*E-mail: zhaojunwei@henu.edu.cn. Fax: (+86) 371 23881589.

ORCID

Junwei Zhao: 0000-0002-7685-1309

Notes

The authors declare no competing financial interest.

ACKNOWLEDGMENTS

This work was supported by the Natural Science Foundation of China (21571048, 21671054, 21301049, U1304208), the Program for Science & Technology Innovation Talents in Universities of Henan Province (16HASTIT001), the Innovation Scientists and Technicians Troop Construction Projects of Henan Province (174100510016), the Foundation of Education Department of Henan Province (16A150027), the Postdoctoral Foundation of Henan Province (20140025), the Foundation of State Key Laboratory of Structural Chemistry (20160016), the 2014 Special Foundation for Scientific Research Project of Henan University (XXJC20140001), the Foundation of Education Department of Henan Province (16A150027), and the Students Innovative Pilot Plan of Henan University (16NA005).

REFERENCES

(1) Fukuda, N.; Yamase, T.; Tajima, Y. *Biol. Pharm. Bull.* **1999**, *22*, 463.

(2) Zhao, Y.; Deng, D. S.; Ma, L. F.; Ji, B.-M; Wang, L. Y. *Chem. Commun.* **2013**, *49*, 10299.

(3) Zheng, S. T.; Zhang, J.; Li, X. X.; Fang, W. H.; Yang, G. Y. *J. Am. Chem. Soc.* **2010**, *132*, 15102.

(4) Heine, J.; Müller-Buschbaum, K. *Chem. Soc. Rev.* **2013**, *42*, 9232.

(5) Descalzo, A. B.; Martínez-Máñez, R.; Sancenón, F.; Hoffmann, K.; Rurack, K. *Angew. Chem., Int. Ed.* **2006**, *45*, 5924.
(6) Cameron, J. M.; Gao, J.; Long, D. L.; Cronin, L. *Inorg. Chem. Front.* **2014**, *1*, 178.
(7) Mal, S. S.; Kortz, U. *Angew. Chem., Int. Ed.* **2005**, *44*, 3777.
(8) Gao, J.; Yan, J.; Beeg, S.; Long, D. L.; Cronin, L. *J. Am. Chem. Soc.* **2013**, *135*, 1796.
(9) Bassil, B. S.; Ibrahim, M.; Al-Oweini, R.; Asano, M.; Wang, Z. X.; van Tol, J.; Dalal, N. S.; Choi, K. Y.; Biboum, R. N.; Keita, B.; Nadjo, L.; Kortz, U. *Angew. Chem., Int. Ed.* **2011**, *50*, 5961.
(10) Huang, L.; Wang, S. S.; Zhao, J. W.; Cheng, L. J.; Yang, G. Y. *J. Am. Chem. Soc.* **2014**, *136*, 7637.
(11) Ma, X.; Yang, W.; Chen, L. J.; Zhao, J. W. *CrystEngComm* **2015**, *17*, 8175.
(12) Li, Y. W.; Li, Y. G.; Feng, Y. H.; Wang, E. B. *Inorg. Chem.* **2009**, *48*, 6452.
(13) Chen, X.; Chen, Y.; Xia, Z.; Hu, H.; Sun, Y.; Huang, W. *Dalton Trans.* **2012**, *41*, 10035.
(14) Li, H. L.; Liu, Y. J.; Zheng, R.; Chen, L. J.; Zhao, J. W.; Yang, G. Y. *Inorg. Chem.* **2016**, *55*, 3881.
(15) Ma, P. T.; Hu, F.; Wan, R.; Huo, Y.; Zhang, D. D.; Niu, J. Y.; Wang, J. P. *J. Mater. Chem. C* **2016**, *4*, 5424.
(16) Wassermann, K.; Dickman, M. H.; Pope, M. T. *Angew. Chem., Int. Ed. Engl.* **1997**, *36*, 13.
(17) Bassil, B. S.; Dickman, M. H.; Römer, I.; von der Kammer, B.; Kortz, U. *Angew. Chem., Int. Ed.* **2007**, *46*, 6192.
(18) Hussain, F.; Conrad, F.; Patzke, G. R. *Angew. Chem., Int. Ed.* **2009**, *48*, 9088.
(19) Ritchie, C.; Moore, E. G.; Speldrich, M.; Kögerler, P.; Boskovic, C. *Angew. Chem., Int. Ed.* **2010**, *49*, 7702.
(20) Hussain, F.; Patzke, G. R. *CrystEngComm* **2011**, *13*, 530.
(21) Hussain, F.; Gable, R.; Speldrich, M.; Kögerler, P.; Boskovic, C. *Chem. Commun.* **2009**, 328.
(22) Ibrahim, M.; Mereacre, V.; Leblanc, N.; Wernsdorfer, W.; Anson, C. E.; Powell, A. K. *Angew. Chem., Int. Ed.* **2015**, *54*, 15574.
(23) Ma, P. T.; Wan, R.; Wang, Y. Y.; Hu, F.; Zhang, D. D.; Niu, J. Y.; Wang, J. P. *Inorg. Chem.* **2016**, *55*, 918.
(24) Artetxe, B.; Reinoso, S.; San Felices, L.; Lezama, L.; Gutiérrez-Zorrilla, J. M.; García, J. A.; Galán-Mascarós, J. R.; Haider, A.; Kortz, U.; Vicent, C. *Chem. - Eur. J.* **2014**, *20*, 12144.
(25) Chen, W.-C.; Li, H.-L.; Wang, X.-L.; Shao, K.-Z.; Su, Z.-M.; Wang, E.-B. *Chem. - Eur. J.* **2013**, *19*, 11007.
(26) Chen, W. C.; Qin, C.; Wang, X. L.; Li, Y. G.; Zang, H. Y.; Shao, Z. K.; Su, Z. M.; Wang, E. B. *Dalton. Trans.* **2015**, *44*, 11290.
(27) Reinoso, S.; Giménez-Marqués, M.; Galán-Mascarós, J.; Vitoria, P.; Gutiérrez-Zorrilla, J. M. *Angew. Chem., Int. Ed.* **2010**, *49*, 8384.
(28) Wang, Y.; Sun, X.; Li, S.; Ma, P.; Niu, J.; Wang, J. *Cryst. Growth Des.* **2015**, *15*, 2057.
(29) Leclerc-Laronze, N.; Haouas, M.; Marrot, J.; Taulelle, F.; Hervé, G. *Angew. Chem., Int. Ed.* **2006**, *45*, 139.
(30) Zhao, J.-W.; Li, H.-L.; Ma, X.; Xie, Z. G.; Chen, L.-J.; Zhu, Y. S. *Sci. Rep.* **2016**, *6*, 26406.
(31) Li, H.-L.; Liu, Y.-J.; Liu, J.-L.; Chen, L.-J.; Zhao, J.-W.; Yang, G.-Y. *Chem. - Eur. J.* **2017**, *23*, 2673.
(32) Chen, W. C.; Yan, L. K.; Wu, C. X.; Wang, X. L.; Shao, K. Z.; Su, Z. M.; Wang, E. B. *Cryst. Growth Des.* **2014**, *14*, 5099.
(33) Pradeep, C. P.; Long, D. L.; Streb, C.; Cronin, L. *J. Am. Chem. Soc.* **2008**, *130*, 14946.
(34) Reinoso, S.; Bassil, B. S.; Barsukova, M.; Kortz, U. *Eur. J. Inorg. Chem.* **2010**, *2010*, 2537.
(35) Sheldrick, G. M. *SHELXS 97*, Program for Crystal Structure Solution; University of Göttingen: Göttingen, Germany, 1997.
(36) Sheldrick, G. M. *SHELXL 97*, Program for Crystal Structure Refinement; University of Göttingen: Göttingen, Germany, 1997.
(37) Pichon, C.; Dolbecq, A.; Mialane, P.; Marrot, J.; Rivière, E.; Sécheresse, F. *Dalton Trans.* **2008**, 71.
(38) Barbieri, G. A. *Atti R. Accad. Naz. Lincei, Mem. Cl. Sci. Fis., Mater. Nat.* **1914**, *11*, 805.
(39) Zhao, J. W.; Li, H. L.; Li, Y. Z.; Li, C. Y.; Wang, Z. L.; Chen, L. J. *Cryst. Growth Des.* **2014**, *14*, 5495.
(40) Li, H. L.; Yang, W.; Wang, X. H.; Chen, L. J.; Ma, J. R.; Zheng, L. W.; Zhao, J. W. *Cryst. Growth Des.* **2016**, *16*, 108.
(41) Yan, J.; Gao, J.; Long, D.-L.; Miras, H. N.; Cronin, L. *J. Am. Chem. Soc.* **2010**, *132*, 11410.
(42) Winter, R. S.; Cameron, J. M.; Cronin, L. *J. Am. Chem. Soc.* **2014**, *136*, 12753.
(43) Yang, W.; Li, H.; Li, Y.; Chen, L.; Zhao, J. *Inorg. Chem. Commun.* **2015**, *60*, 71.
(44) Xue, H.; Zhang, Z.; Pan, R.; Yang, B.-F.; Liu, H.-S.; Yang, G.-Y. *CrystEngComm* **2016**, *18*, 4643.
(45) Chen, W.-C.; Qin, C.; Wang, X.-L.; Wu, C.-X.; Li, Y.-G.; Zang, H.-Y.; Shao, K.-Z.; Su, Z.-M.; Wang, E.-B. *CrystEngComm* **2016**, *18*, 2820.
(46) Liang, Y.; Li, S.; Yang, D.; Ma, P.; Niu, J.; Wang, J. *J. Mater. Chem. C* **2015**, *3*, 4632.
(47) Dickins, R. S.; Aime, S.; Batsanov, A. S.; Beeby, A.; Botta, M.; Bruce, J. I.; Howard, J. A. K.; Love, C. S.; Parker, D.; Peacock, R. D.; Puschmann, H. *J. Am. Chem. Soc.* **2002**, *124*, 12697.
(48) Kuriki, K.; Koike, Y. *Chem. Rev.* **2002**, *102*, 2347.
(49) Koester, C. J.; Snitzer, E. *Appl. Opt.* **1964**, *3*, 1182.
(50) Yajima, H.; Kawase, S.; Sekimoto, Y. *Appl. Phys. Lett.* **1972**, *21*, 407.
(51) Mears, R. J.; Reekie, L.; Poole, S. B.; Payne, D. N. *Electron. Lett.* **1985**, *21*, 738.
(52) Veith, M.; Belot, C.; Huch, V.; Cui, H. L.; Guyard, L.; Knorr, M.; Wickleder, C. *Eur. J. Inorg. Chem.* **2010**, *2010*, 879.
(53) Liu, J. C.; Yu, J.; Han, Q.; Wen, Y.; Chen, L. J.; Zhao, J. W. *Dalton Trans.* **2016**, *45*, 16471.
(54) Abdelhameed, R. M.; Carlos, L. D.; Silva, A. M. S.; Rocha, J. *Chem. Commun.* **2013**, *49*, 5019.
(55) Boens, N.; Qin, W.; Basarić, N.; Hofkens, J.; Ameloot, M.; Pouget, J.; Lefèvre, J.-P.; Valeur, B.; Gratton, E.; vandeVen, M.; Silva, N. D.; Engelborghs, Y.; Willaert, K.; Sillen, A.; Rumbles, G.; Phillips, D.; Visser, A. J. W. G.; van Hoek, A.; Lakowicz, J. R.; Malak, H.; Gryczynski, L.; Szabo, A. G.; Krajcarski, D. T.; Tamai, N.; Miura, A. *Anal. Chem.* **2007**, *79*, 2137.
(56) Zhang, Y.; Gong, W.; Yu, J.; Pang, H.; Song, Q.; Ning, G. *RSC Adv.* **2015**, *5*, 62527.
(57) Chen, L. J.; Zhang, F.; Ma, X.; Luo, J.; Zhao, J. W. *Dalton Trans.* **2015**, *44*, 12598.
(58) Ritchie, C.; Baslon, V.; Moore, E. G.; Reber, C.; Boskovic, C. *Inorg. Chem.* **2012**, *51*, 1142.
(59) Zhao, J. W.; Luo, J.; Chen, L. J.; Yuan, J.; Li, H. Y.; Ma, P. T.; Wang, J. P.; Niu, J. Y. *CrystEngComm* **2012**, *14*, 7981.

DOI: 10.1021/acs.cgd.7b00539
Cryst. Growth Des. 2017, 17, 3917−3928